A MODEL OF BASAL HYDROLOGIC NETWORKS AND EFFECTIVE STRESS BENEATH AN ICE SHEET

by

SARA SABRINA PAPAMARCOS

A THESIS

Presented to the Department of Geological Sciences
and the Graduate School of the University of Oregon
in partial fulfillment of the requirements
for the degree of
Master of Science

March 2012

THESIS APPROVAL PAGE

Student: Sara Sabrina Papamarcos

Title: A Model of Basal Hydrologic Networks and Effective Stress Beneath an Ice Sheet

This dissertation has been accepted and approved in partial fulfillment of the requirements for the Master of Science degree in the Department of Geological Sciences by:

Alan Rempel	Chair
Joshua Roering	Member
Eugene Humphreys	Member

and

Kimberly Andrews Espy	Vice President for Research & Innovation/Dean of the Graduate School

Original approval signatures are on file with the University of Oregon Graduate School.

Degree awarded March 2012

THESIS ABSTRACT

Sara Sabrina Papamarcos

Master of Science

Department of Geological Sciences

March 2012

Title: A Model of Basal Hydrologic Networks and Effective Stress Beneath an Ice Sheet

Subglacial processes that control the water pressure and flow determine the large-scale behavior of the overlying ice by regulating basal resistance. We implement a model in which a steady-state subglacial conduit system is surrounded by fully-saturated porous media. We investigate branching in this system at fixed angles of 15°, 30° and 45° to the direction of ice flow and further assess these systems by calculating the hydraulic potential gradient to determine conduit flow path. We solve our governing equations for porous media flow and allow ice infiltration of the pore space to occur at a critical effective stress $N_{infiltration}$. For low values of $N_{infiltration}$, ice infiltration of sediment allows these conduits to follow their original paths. Where insufficient ice infiltration occurs, the conduit path instead lies parallel to the direction of ice flow. Our results speak to the importance of incorporating small-scale processes into models of subglacial hydrologic networks.

CURRICULUM VITAE

NAME OF AUTHOR: Sara Sabrina Papamarcos

GRADUATE AND UNDERGRADUATE SCHOOLS ATTENDED:

University of Oregon, Eugene
Brown University, Providence, RI

DEGREES AWARDED:

Master of Science in Geological Sciences, 2012, University of Oregon
Bachelor of Science in Geology-Mathematics/Physics, 2005, Brown University

AREAS OF SPECIAL INTEREST:

Antarctica, Ice Physics, Hydrogeology

PROFESSIONAL EXPERIENCE:

Research in Thermal Conductivity of Ice Clathrates, 2005, Brown University

GRANTS, AWARDS, AND HONORS:

Graduate Teaching Fellowship, 2009 to present

First Place, National Science Olympiad, 2004, Awesome Aquifers Category

ACKNOWLEDGMENTS

I thank Professor Alan Rempel for his assistance in the preparation of this manuscript and for his support and guidance as my advisor. Additionally, I thank Josh Roering and Gene Humphreys for their guidance as members of various committees during my time at the University of Oregon. Special thanks are due to Schuyler Redding, whose support during the writing of this thesis was crucial to its completion. I also thank Outi and Andrew Papamarcos for their endless support.

TABLE OF CONTENTS

LIST OF FIGURES

Figure Page

Figure Page

LIST OF TABLES

Table Page

CHAPTER I

INTRODUCTION

Subglacial processes determine the large-scale behavior of the overlying ice sheet by regulating basal resistance. Resistance occurs as ice deforms around obstacles and as debris is dragged along the bed. Much attention has been focused on the relationship between the water present at the base of the ice sheet and the basal resistance because this basal water is thought to reduce friction by drowning out smaller roughness elements (Lliboutry, 1964; Schoof, 2005) and exerting a pressure that partly offsets the weight of the overlying ice (Kamb, 1991).

Despite this seemingly simple relationship between basal water and basal resistance, it is difficult to ascertain basal conditions from the data available. Complete 300 m resolution velocity maps are newly available for Antarctica (Rignot et al., 2011), but inverting for basal conditions requires the interpretation of a hydrologic model. Synthetic Aperture Radar (SAR) methods have sucessfully mapped the bed, though difficulty arises in trying to distinguish roughness from wetness at the bed-ice interface (Jezek et al., 2011) because the scale of the signal is the same as that of the error. Direct measurements of bed conditions are limited to point-data from boreholes, which have been used to measure properties like basal water pressure and hydraulic conductivity of subglacial sediments (Fountain and Walder, 1998). Dye-tracing has been used to measure discharge and mean flow velocity in systems with known hydraulic geometry (Nienow et al., 1996), though this method is difficult to implement in an ice sheet setting.

Lacking an explicit way to determine subglacial hydrology, it therefore becomes necessary to model the types of hydrologic networks we see evidence for: linked cavities, conduits, and porous media flow. Linked cavities provide a viable explanation for the surging behavior seen in hard-bedded glaciers like Variegated Glacier (Kamb et al., 1985) and are substantiated by subsequent borehole observations of water level and pressure (Flowers, 2010). Studies of eskers formed under the Laurentide and Eurasian ice sheets indicate past arborescent networks of conduits, where eskers are typically associated with rigid beds and are comprised of coarser sediment (Clark and Walder, 1994). Till layers of up to ten meters thick range from continuous sheets to discontinuous patches and are commonly observed beneath ice sheets, whereas these patches are less common beneath valley glaciers (Fountain and Walder, 1998).

Presently, many models focus on the linked cavity system of a hard-bedded glacier (Creyts and Schoof, 2009; Schoof, 2010; Hewitt, 2011). These studies model water flow through macroporous sheets, which act as thin, widespread conduits and tend to average the subglacial processes such that a physical sense of what happens where the ice contacts the bed is obscured. My model is distinct from many recent models of subglacial hydrology in that it focuses on soft-bedded ice sheets where water flows through conduits incised in till, a notion supported by previous studies of such conduits (Fountain and Walder, 1998; Walder and Fowler, 1994). These conduits are in turn supplied by water from their surroundings by porous media flow, a well-documented process. In modeling water flow through the till bed, we capture the conditions of the bed-ice interface in hopes of providing physical insight into the location of conduits

beneath the ice sheet and their effect on the stress conditions in the surrounding bed.

Additionally, my model strives to address the rigid structure of networks seen in previous modeling efforts in order to produce networks that are more arborescent in nature, resulting in branched conduits. The primary control on this structure is the dominant potential gradient imposed by variations in elevation of the ice surface, which drive ice flow and cause modeled conduits to align parallel to ice flow in rigid lines (Hewitt, 2011; Pimentel and Flowers, 2011). An alternative strategy used to impose arborescent networks requires water flow to occur along a set grid, where water must flow between nodes at 45 degrees to the direction of ice flow (Schoof, 2010). My model bridges the middle ground between these methods by requiring the position of the conduit beneath the ice sheet to depend on the strong ice thickness gradient while allowing other physical factors to produce deviations in this flow direction.

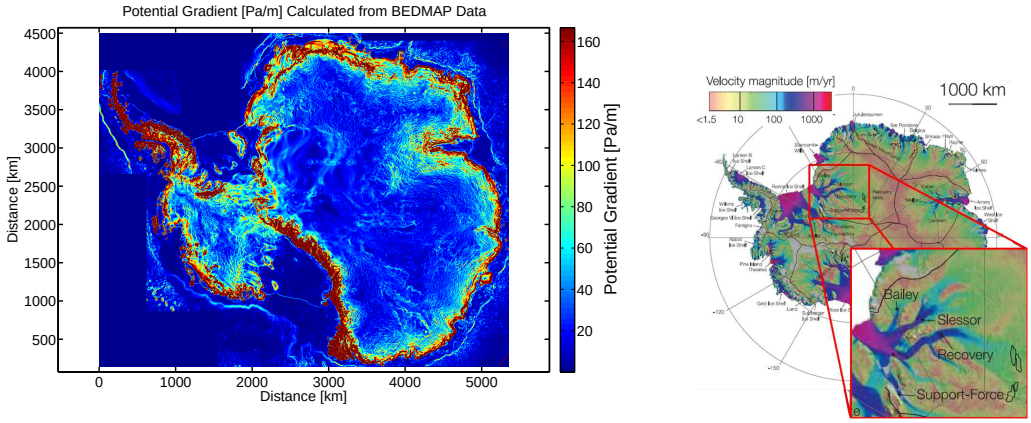

(a) (b)

FIGURE 1. (a) Map of Antarctica with corresponding ψ values calculated using data from BAS (2000), (b) Location of Recovery Basin imposed on velocity map of Antarctica modified from Rignot et al. (2011).

Understanding both the steady-state and transient conditions at the bed is crucial to understanding the interaction between subglacial processes and the sliding rate of the overlying ice sheet. While transient events are frequently studied due to the notion that flooding a system with water causes surging in the overlying ice sheet, steady-state studies provide insight into the nature of long-term trends in sliding. This study therefore focuses on conditions typical of the East Antarctic ice sheet, wherein a steady-state network of conduits might be expected due to the slow pace of the ice sheet and the low rate of water input. Figure 1 shows a map that we generated using BEDMAP data provided by the British Antarctic Survey (BAS) to show the driving potential gradient for Antarctica and focuses on the Recovery Basin that we base our parameter estimates on. We examine how a conduit system could organize itself such that arborescent branches would remain in a steady-state configuration as well as how local bed properties might affect the location of the conduit and the stress conditions in the surrounding bed. Using these results, we examine the implications of how varying bed properties influence the bed and conduit effective stress as well as the conditions under which a steady-state conduit network with a set geometry may exist.

CHAPTER II

DRAINAGE MODELS

We consider an ice sheet sliding over a till bed with porous media flow draining meltwater generated at the ice-bed interface to adjacent conduits cut into the till. Here, we present the main model and the governing equations, for a more detailed derivation refer to the appendices. The coordinate system and boundary conditions used in the model are designed to examine branching that occurs symmetrically around a central conduit that is supplied by meltwater from both sides before branching and whose subsequent branches are supplied only by meltwater from between the central and far hydrologic divides. Ice flows in the y-direction, with the horizontal component x measured as positive from the central conduit toward a hydrologic divide (Figure 2). The gradient imposed by changes in the surface elevation z_s is directed only in the y-direction. Additional changes in bed elevation z_b occur in x and y, contributing to the total hydraulic potential at depth $z < z_b$,

$$\Phi = P(z_b) + \rho_w g(z_b - z) + \delta P(z) \tag{2.1}$$

where $P(z_b)$ is the water pressure at z_b, ρ_w is the density of water, g is the gravitational acceleration, and δP is the non-hydrostatic component of water pressure at some depth $z < z_b$. The datum $z = 0$ is located at first contact between ice and the underlying till. We assume that ice can infiltrate into the till and fill the pore space such that the bulk density of ice-saturated till is written in terms of the porosity of till ϕ, the density of till ρ_t, and the density

of ice ρ_i as $\rho_b = \phi\rho_i + (1-\phi)\rho_t$. Water flows down a potential gradient $\nabla\Phi$ that consists of a geometrical potential

$$\psi = -\rho_i g \nabla z_s - (\rho_w - \rho_b) g \nabla z_b, \tag{2.2}$$

and the gradient in effective stress N so that

$$-\nabla\Phi = -\psi - \nabla N \tag{2.3}$$

where ρ_i is the density of ice and N is the overburden pressure less the water pressure at z_b. We examine steady-state configurations where all water present at the base of the ice sheet results from melting at the ice-bed interface. We assume that conduits form along the highest potential gradients, and by calculating the potental gradient for the conduit at various angles, we determine the path of the conduit through a till bed. In preliminary work, we found that network geometries are dominated by the strong gravitational gradient imposed by changes in ice thickness but that when conduits were forced to branch, regions of high effective stress exist between branches. Work by Rempel (2009) states that at high effective stress, ice infiltrates into the pore space between sediment, possibly providing a mechanism for keeping branches of a conduit network separate by causing the potential gradient to deviate from the direction of the ice surface gradient.

Porous Media Flow

Water flows through the till layer of uniform thickness h_{sed}, bounded by the ice above and impermeable bedrock below. We use a depth-averaged

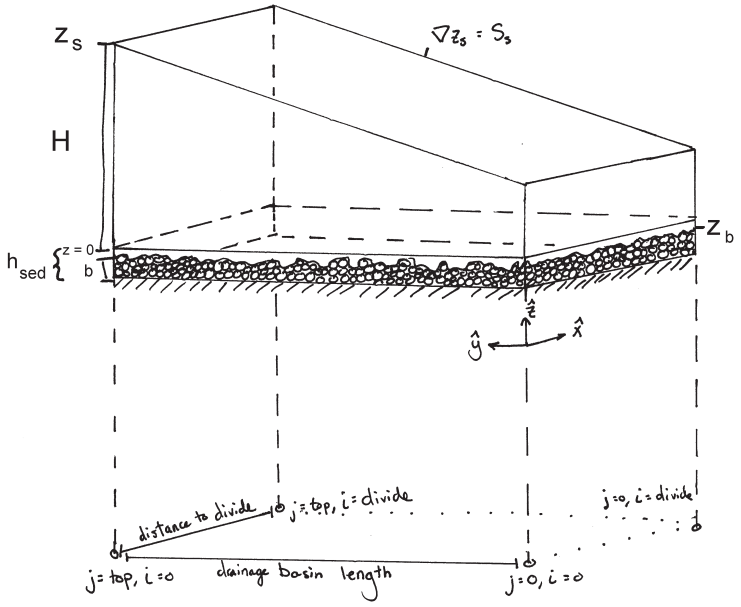

FIGURE 2. Rough diagram showing parameter definitions as well as how the finite difference model relates to the physical boundaries of the system.

equation for Darcy flow to quantify porous media flow and determine the effective stress at the bed. We are interested in conditions typical of ice sheets like the East Antarctic Ice Sheet, where what little surface melting that occurs during the summer is expected to freeze near the surface so the water balance at the bed does not involve significant external inputs. We estimate the divergence in water flux at the ice-bed interface using an intermediate melt rate of $\dot{m} =$ 5 mm/yr where water flows along the hydraulic potential gradient described previously (2.3). The rate of flow is proportional to the transmissivity T and it diverges in response to the melting so that

$$\dot{m} = \nabla \cdot \left(\frac{T}{\rho_w g} \left[\psi + \nabla N \right] \right). \tag{2.4}$$

We determine this melting rate using a heat balance that accounts for local heat fluxes due to geothermal heating, frictional heating, and conduction of heat away from the bed through the ice sheet. When N exceeds the critical effective stress of $N_{infiltration}$, the transmissivity changes as a function of effectives stress,

$$T = T_o + \lambda(N - N_{infiltration}) \text{ for } N > N_{infiltration} \tag{2.5}$$

due to infiltration of ice into the till where the negative constant λ limits the area through which basal meltwater can flow. At low effective stress, the transmissivity is constant at

$$T = T_o \text{ for } N \leq N_{infiltration} \tag{2.6}$$

We solve our governing equation (2.4) using a finite difference method where a zero-flow condition is applied as the boundary condition at hydrologic divides such that depth-averaged flow velocity across the divide $\overline{u_x} = 0$ where

$$\overline{u} = \frac{T}{\rho_w g} \left(\psi + \nabla N\right). \tag{2.7}$$

At the lower boundary we assume a constant effective stress equal to that at the outlet of the conduit, indicating that our model terminates in either a change of transport mechanism or a site of water storage, like a subglacial lake. At the upper boundary, we specify a constant Darcy flow rate c_t such that $\overline{u}b \cdot \widehat{y} = c_t$ to simulate porous media flow down into the drainage basin from a collection area above. The conduit provides a final condition in the model, where the node nearest the location of the conduit retains the value of effective stress

calculated by our conduit flow model for that location. We assume that where porous media flow occurs near a conduit, the portion of the flow perpendicular to the conduit feeds this system. We calculate this meltwater flux from the till surrounding the conduit using the results of the finite difference model where the supply of melt to a given section of conduit per meter of conduit Ω is defined as the component of melt perpendicular to the conduit

$$\Omega = |\overline{u}|bsin(\theta), \tag{2.8}$$

where θ is the angle between the conduit axis and the direction of Darcy flow.

Conduit Flow

Subglacial conduits cut into the till result from a balance between inward viscous creep of the ice surrounding the conduit and melting due to turbulent heating. Water flows through these conduits from high to low pressure and draws in water from the surrounding till. We assume these conduits form a dendritic network and exhibit a consistent cross-sectional shape, which dictates the value of a frictional constant F. We formulate our governing equations for conduit flow based on Nye's 1976 discussion of flow in glacial tunnels (see also Hewitt, 2011), where we consider conservation of water mass (2.9), a balance between creep closure and turbulent melting of the conduit walls (2.10), a turbulent water flow law based on the Gauckler-Manning formula for mean velocity (2.11), and an energy balance that determines the conduit wall melting rate in an isothermal system (2.12). We solve these equations,

$$\frac{\partial Q}{\partial s} + \frac{\partial S}{\partial t} = \frac{M}{\rho_w} + \Omega \tag{2.9}$$

$$\frac{\partial S}{\partial t} = \frac{M}{\rho_i} - \frac{SN_c}{\eta_i} \tag{2.10}$$

$$\frac{Q^2}{S^{8/3}} F = \frac{Q^2}{S^{8/3}} \left(\frac{S}{R^2}\right)^{2/3} \rho_w g n'^2 = \psi - \frac{\partial N}{\partial s} \tag{2.11}$$

$$ML = Q(\psi - \frac{\partial N_c}{\partial s}), \tag{2.12}$$

for steady-state conditions, where the cross-sectional area S does not vary in time t. Here Q is the volumetric flux, M is the melting rate of the conduit walls, Ω is the component of water flowing to the conduit from the surrounding bed calculated using Darcy's law, η_i is the ice viscosity, R is the hydraulic radius, n' is Manning's roughness coefficient, $\widehat{s}$ is the flow direction of the conduit, and L is the latent heat of ice. We combine (2.9), (2.10),(2.11), and (2.12) to determine the steady-state form of the changes in Q and N along the direction of conduit flow as

$$\begin{aligned} \frac{dQ}{ds} &= \frac{M}{\rho_w} + \Omega \\ &= \left(\frac{F}{L}\right)^{3/11} \left(\frac{N_c \rho_i}{\eta_i}\right)^{8/11} \left(\frac{Q^{9/11}}{\rho_w}\right) + \Omega, \end{aligned} \tag{2.13}$$

$$\begin{aligned} \frac{dN_c}{ds} &= \frac{ML}{Q} - \psi \\ &= \left(\frac{\rho_i N_c}{\eta_i}\right)^{8/11} \left(\frac{F}{L}\right)^{3/11} \left(\frac{Q^{9/11}}{Q}\right) L - \psi \\ &= \left(\frac{F^{3/11}}{Q^{2/11}}\right) \left(\frac{N_c \rho_i L}{\eta_i}\right)^{8/11} - \psi. \end{aligned} \tag{2.14}$$

Using an ODE integrator to solve these equations, we determine the hydraulic gradient for possible channel orientations measured by angle from the y-axis. We choose the starting conditions at the base of the model domain as $N_{co} = 50$ kPa and $Q_o = 1$ m^3/s within the range of values presented by Hewitt (2011), who uses a similar formulation for conduit flow. For intuition, using constant initial values implies a steady cross-sectional area at the base of the model domain of ≈ 9.7 m^2.

Effective Stress Profiles for Specified Conduit Angles

Initially we calculate the effective stress profile in the conduit and the surrounding till for angles that conduits have been set to in previous studies: 0°, 15°, 30°, and 45°. We examine both the change in average effective stress and in conduit effective stress over the length of our drainage basin as well as the volumetric flux in the conduit and the average porous media flux across the drainage basin at the same location. The results of these simulations show the requisite effective stress profile for this configuration of conduit under steady-state conditions. As we expect, when the conduit is maintained at steeper angles, a higher effective stress drop occurs over the course of the conduit. A region of low effective stress between the conduit and the central divide indicates the presence of high-pressure fluid between symmetrical branches that occur as we describe.

We then use these geometries to provide the starting bed conditions for a conduit that follows the highest total potential gradient. We determine this path by first calculating the potential gradients for a range of angles and selecting the maximum value.

CHAPTER III

RESULTS

In exploring the different configurations of branching in subglacial conduits beneath ice sheets, we first evaluate the conditions required for branching of conduits at specified angles. Using these effective stresses and ice-infiltration depths as initial conditions for further iterations of the model's governing equations, we then implement our method for determining the path the conduit would take. As porous media flow is calculated as the solution to Poisson's equation, this portion of our model is guaranteed to converge on a unique solution for any conduit geometry where $T = T_o$. We also expect the existence of a solution for the case in which T is a function of N. The conduit follows the path where the fastest downstream flow occurs due to alignment with the highest potential gradient. In our model, we assume that the conduit system is in steady-state and thus implementing our model to determine the optimum conduit path determines the sustainability of the conduit system as initially calculated. When examining the figures presented, it is important to recall that for all conduit configurations, branching is forced to occur 700 m from the head of the glacier. We will vary the effective stress at which ice infiltration occurs $N_{infiltration}$ in order to guage the highest potential gradient at the base of the ice sheet. From (2.5) we know that varying $N_{infiltration}$ while holding λ constant will affect the depth to which ice infiltrates. The critical effective stress is determined by the typical pore size in the till, with larger pores resulting in lower values of $N_{infiltration}$. Thus the physical meaning of altering this value

is to coarsen or fine the till bed as we decrease or increase the $N_{infiltration}$ respectively.

Conduit Branching at Specified Angles

By initially specifying the angle at which branching occurs in our model, we evaluate the conditions that the conduit network in this configuration would require if it were maintained under steady-state condition given the conditions described in Table 1. The initial rate of water supply to the conduit Ω is estimated by assuming that some component of the water generated by melting at the ice-bed interface travels parallel to the conduit and thus does not contribute to Ω and because Q_o is large relative to the porous media influx from the surrounding bed, this assumption does not significantly alter our resulting effective stress calculations. In, subsequent iterations of the model, Ω is calculated as previously described (2.8). For all angles, large regions of low effective stress (Figure 3) indicate high pressure fluid where the influence of the conduit does not sufficiently drain the till. Around each conduit, we show the corresponding depths to which ice has infiltrated (Figure 4) in order to illustrate that an ice fringe lines the conduit in cases where $N_{infiltration}$ is low. As we vary $N_{infiltration}$ (Figure 5, we see that the depth to which ice penetrates the till around the conduit decreases until only a thin fringe remains at the head of the conduit where the effective stress is highest for $N_{infiltration} = 60$ kPa. Figure 6 presents a closer look at the pattern of porous media flow. We note that where the till is far from the conduit, porous media flow aligns with the direction of ice flow. The maximum magnitude of z_b that we find for any value of $N_{infiltration}$ is

$\approx$ -0.16 m, indicating that this λ value will not result in deep penetration of the till.

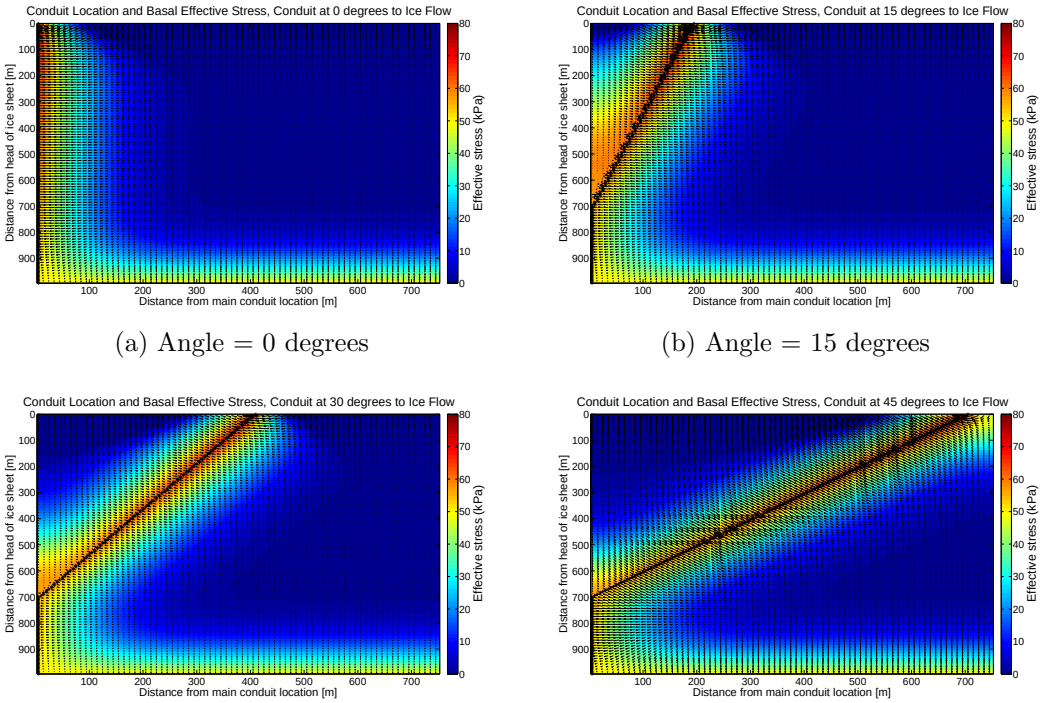

(a) Angle = 0 degrees

(b) Angle = 15 degrees

(c) Angle = 30 degrees

(d) Angle = 45 degrees

FIGURE 3. Graph of the effective stress in the drainage basin where $N_{infiltration} = 10$ kPa. The conduit is indicated as a black cross and the direction of porous media flow is indicated by the vector field. Where the till is far from the conduit, low effective stresses prevent ice infiltration into the till whereas the regions nearest the conduit experience high effective stress and infiltration of ice into the till to a depth shown in Figure 4.

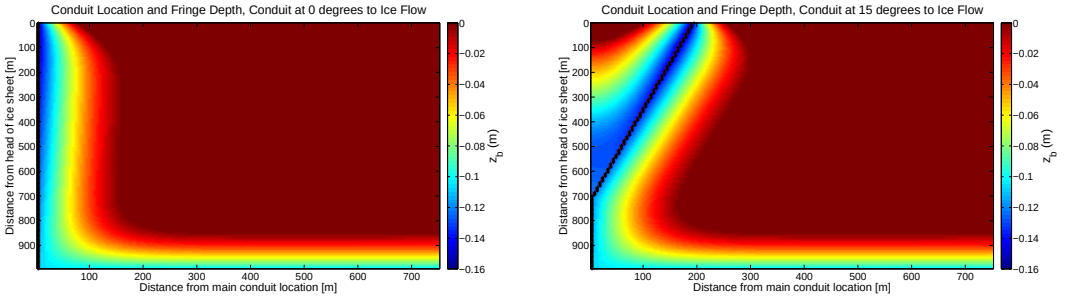

(a) Angle = 0 degrees

(b) Angle = 15 degrees

(c) Angle = 30 degrees

(d) Angle = 45 degrees

FIGURE 4. Graph of the ice-infiltration depths in the drainage basin where $N_{infiltration} = 10$ kPa. The conduit is indicated as a black cross and the effective stress in the drainage basin is shown in Figure 3.

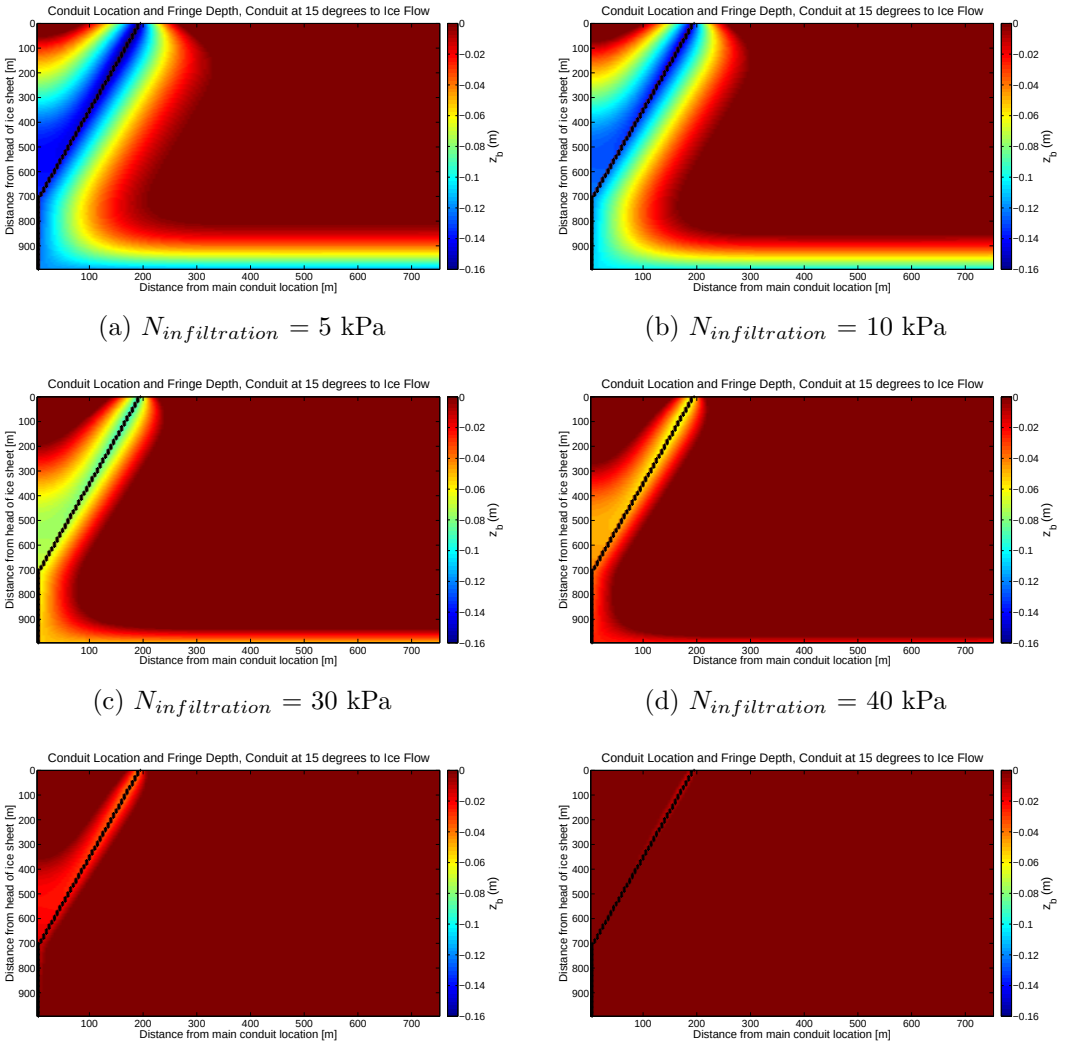

(a) $N_{infiltration} = 5$ kPa

(b) $N_{infiltration} = 10$ kPa

(c) $N_{infiltration} = 30$ kPa

(d) $N_{infiltration} = 40$ kPa

(e) $N_{infiltration} = 50$ kPa

(f) $N_{infiltration} = 60$ kPa

FIGURE 5. Graph of the ice-infiltration depths in the drainage basin for different vaules of $N_{infiltration}$. The conduit is indicated as a black cross and the direction of porous media flow is indicated by the vector field. Where the till is far from the conduit, low effective stresses prevent ice infiltration into the till whereas the regions nearest the conduit experience ice infiltration of up to $z_b \approx -0.16$ m.

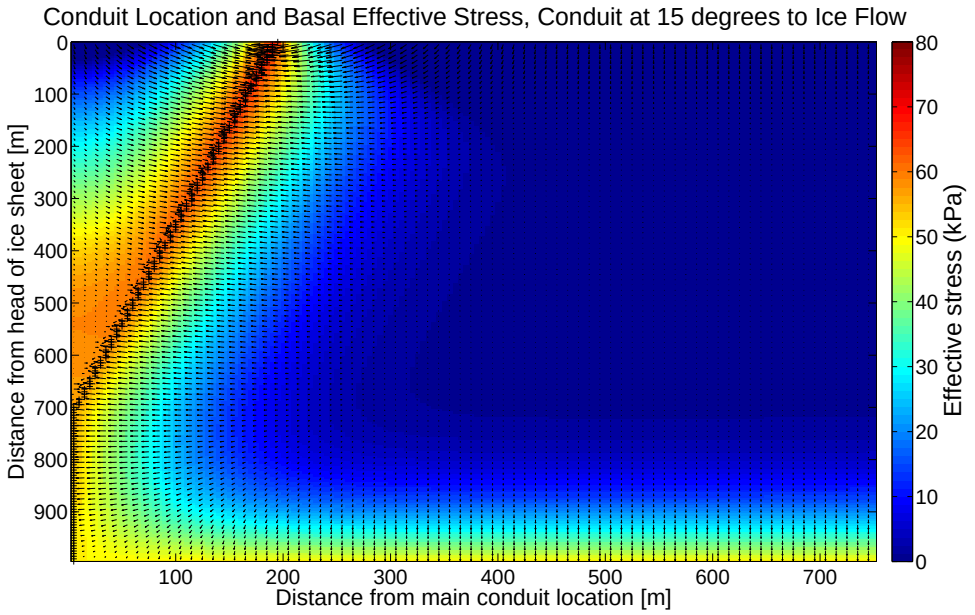

FIGURE 6. Graph of the effective stress in the drainage basin for a set angle of 15° where $N_{infiltration} = 10$ kPa. Low effective stresses indicate high fluid pressure. The conduit is indicated as a black cross and the direction of porous media flow is indicated by the vector field. Where the till is far from the conduit, porous media flow aligns with the direction of ice flow whereas near the conduit, flow feeds the conduit system.

Parameter		**Values**
Rate of Ice Infiltration	λ	-2.6 $\cdot 10^{-10}$ (m^2/s)/Pa
Sediment thickness	b	1 (m)
Geometric factor for circular conduit	F	650 (kg $m^{-8/3}$)
Potential gradient due to ice thickness gradient	ψ	19 (Pa/m)
Conduit effective stress at outlet	N_{cf}	50 kPa
Volumetric flux at outlet	Q_f	1 m^3/s
Conduit branching angles		0°, 15°, 30°, 45°
Critical effective stress for ice infiltration	$N_{infiltration}$	5 - 60 kPa

TABLE 1 Table of initial parameters specified in calculating the initial effective stress profile of conduits branching at predetermined angles.

For higher branching angles, porous media flow acts against the ice surface elevation gradient in order to reach the conduit. Where negative effective stresses occur, we increase the transmissivity of the porous media in order to emulate the effects of ice-bed separation and film flow. As the transmissivity of these regions is increased, water is evacuated more easily and the overall gradient in effective stress in these regions is reduced (Figure 7). One effect of increasing the transmissivity to account for film flow can be seen in the high pressure gradients that line the boundary between regions of higher and lower transmissivity. Overall, the change in transmissivity we apply here relieves some of the high fluid pressure in these zero effective stress regions. We use this technique to gather insight into the nature of the regions high fluid pressure, but we do not implement this procedure in our subsequent modeling efforts for simplicity in the selection of the conduit path.

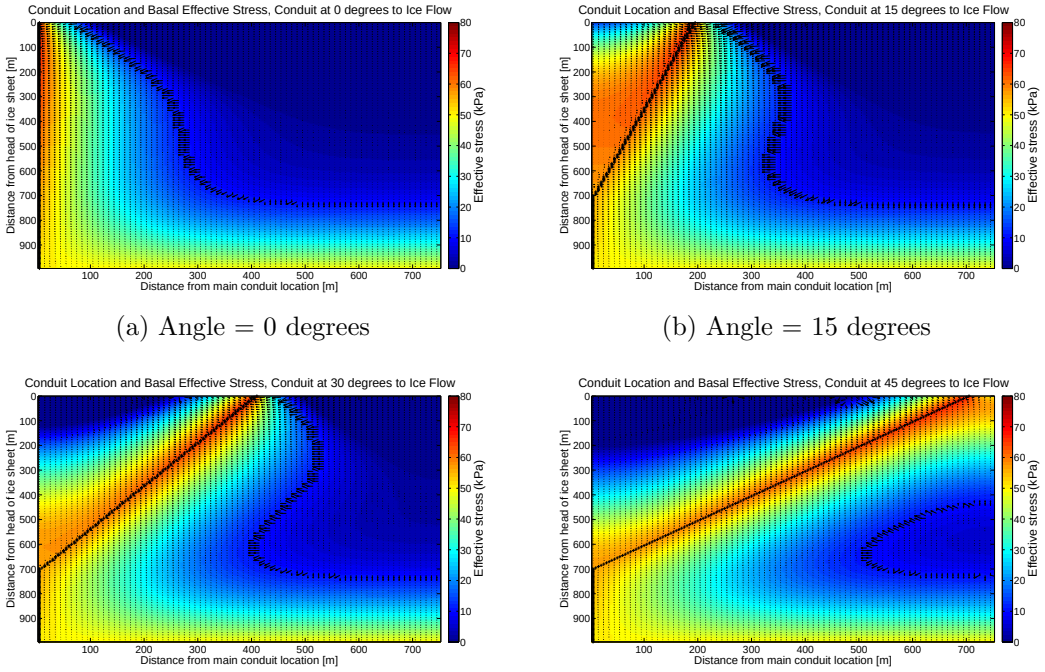

(a) Angle = 0 degrees

(b) Angle = 15 degrees

(c) Angle = 30 degrees

(d) Angle = 45 degrees

FIGURE 7. Graph of the effective stress in the drainage basin where $N_{infiltration} = 10$ kPa and the transmissivity of regions of zero effective stress or below is increased by a factor of five. The conduit is indicated as a black cross and the direction of porous media flow is indicated by the vector field.

Conduit Path Selection Using Bed Conditions Calculated At Specified Angles

Using the effective stress, ice infiltration depth, and transmissivity results calculated by requiring conduit branching to occur at specified angles, we tested the ability of the system to maintain the predetermined geometry. In evaluating these initial inputs, we used our model to determine the highest potential gradient available and found that the highest potential gradient remained fixed along the chosen path. The results of this path selection process include incorporation of the porous media flow rate in the bed into the calculation of water supplied to the conduit as opposed to the initial estimation of Ω. These

new effective stress profiles thus give a more realistic view of the steady-state conduit network.

We evaluate conduit network geometry for multiple values of $N_{infiltration}$ by graphing both the average effective stress and the conduit effective stress (Figure 8). In order to interpret these curves, we show the results of the conduit path selection model associated with the $N_{infiltration} = 5$, 30, and 60 kPa alongside the graphed averages (Figure 9). By examining these figures we see that for high critical effective stress values, insufficient ice penetrates the area around the conduit, causing the highest potential gradient to lie along a shallower angle for $N_{infiltration} = 60$ kPa. At 700m, we observe that branching occurs and the lowest value of $N_{infiltration}$ produces a higher overall effective stress as a result of the decrease in the transmissivity of the region due to ice infiltration and higher effective stress gradients are required to drive Darcy flow toward the conduit.

Where $N_{infiltration} \leq 10$ kPa, we see the tendency of the highest potential gradient to remain along the predetermined path for conduits surrounded by infiltrated till as shallow as, $z_b \leq -0.06$ m. However, the conduits continue to remained branched when the ice between the conduit and the central divide infiltrated to a depth of $z_b \leq -0.01$ m instead of reverting to an angle of $0°$. In systems where porous media surrounds the conduit network, we see that the magnitude of change in ice penetration depth greatly influences the hydraulic gradient such that water may even flow against the gradient in the ice surface elevation. We see this effect in our initial evaluations of the effective stress profile for a conduit system branching at $45°$ (Figure 11) where for stable branches at higher angles, porous media flow acts against the gradient in surface

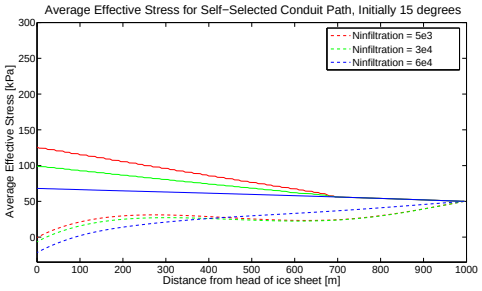

(a) Angle = 15 degrees

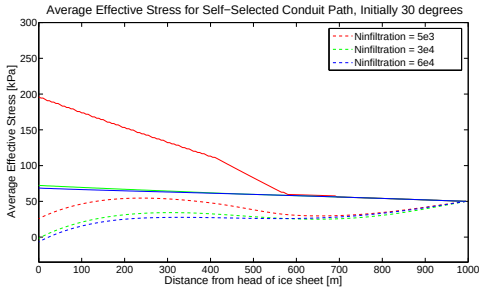

(b) Angle = 30 degrees

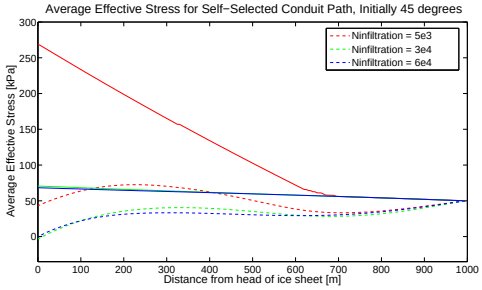

(c) Angle = 45 degrees

FIGURE 8. Graph of the conduit effective stress (solid) and average effective stress in the surrounding bed (dashed) for $N_{infiltration}$ = 5, 30, and 60 kPa after the conduit has selected its path using the three initially branched profiles. As we did not see variation from the conduit system aligned with the gradient in ice surface elevation, we do not include a graph here.

elevation in the region adjacent to the conduit. For hard bedded glaciers, the small density difference between water and ice ensures that $\rho_i g >> (\rho_w - \rho_i)g$ so that the gradient in the glacier surface exerts primary control on the hydraulic gradient in the presence of water. With a soft-bedded glacier that is infiltrated into the till beneath, the average density of ice-infiltrated till is such that $|\rho_i g| \sim |(\rho_w - \rho_i\phi - \rho_t(1-\phi))g|$ so that the gradients in the bed surface elevation and gradients in the glacier surface are of comparable importance for driving water flow. In our model, this helps to limit the degree to which conduits are forced to align in the direction of glacier flow.

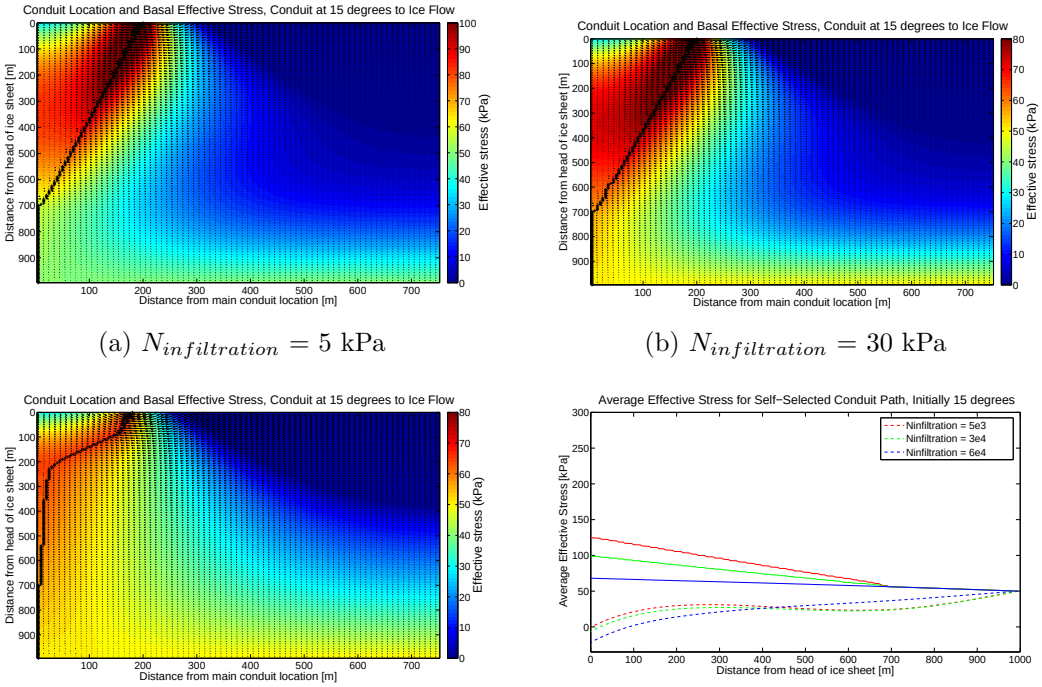

(a) $N_{infiltration}$ = 5 kPa

(b) $N_{infiltration}$ = 30 kPa

(c) $N_{infiltration}$ = 60 kPa

(d) Angle = 15 degrees

FIGURE 9. Graphs of the effective stress in the drainage basin after the conduit has selected its path after setting the initial conduit path to 15° are shown for $N_{infiltration}$ = 5 (a), 30 (b), and 60 kPa (c). The conduit is indicated as a black cross and the direction of porous media flow is indicated by the vector field. For comparison, we show the conduit effective stress (solid) and average effective stress in the surrounding bed (dashed) for these scenarios (d), where $N_{infiltration}$ = 5, 30, and 60 kPa are indicated by red, green, and blue lines respectively.

CHAPTER IV

DISCUSSION

Our results show that, in the absence of physical barriers, the highest potential gradient lies along the path parallel to ice flow. However, configurations like that of a conduit branching even as low as 15° in this snapshot view of the steady-state system build fluid pressure high enough to cause flotation of ice between the conduits. If a significant portion of the bed between two conduit branches reached flotation, this lack of basal friction might allow sliding to occur more rapidly and potentially destroy the conduit network. Conversely, the high effective stress between the two branches as well as the infiltration of ice between the branches (Figure 5), in the region of the central divide, is promising for stable low-angle branching. For high $N_{infiltration}$ values, we see that when the conduit path is self-selected, the conduit migrates toward the central divide until the smaller angle results in a high effective stress that allows the ice to penetrate to a depth of 0.005 m, where this lower angle of conduit can be maintained (Figure 10).

In preliminary efforts, we found that till-bedded models of subglacial hydrologic networks that did not incorporate ice infiltration always aligned with the potential gradient imposed by the changing ice surface elevation unless allowed an imposed perturbation wherein the form of the network was determined by the perturbation and did not follow the highest potential gradient. Our results therefore imply that the natural controls on ice infiltration may play an important role in the establishment of branched conduit networks beneath ice sheets. These evaluations of the gradient in hydraulic potential are

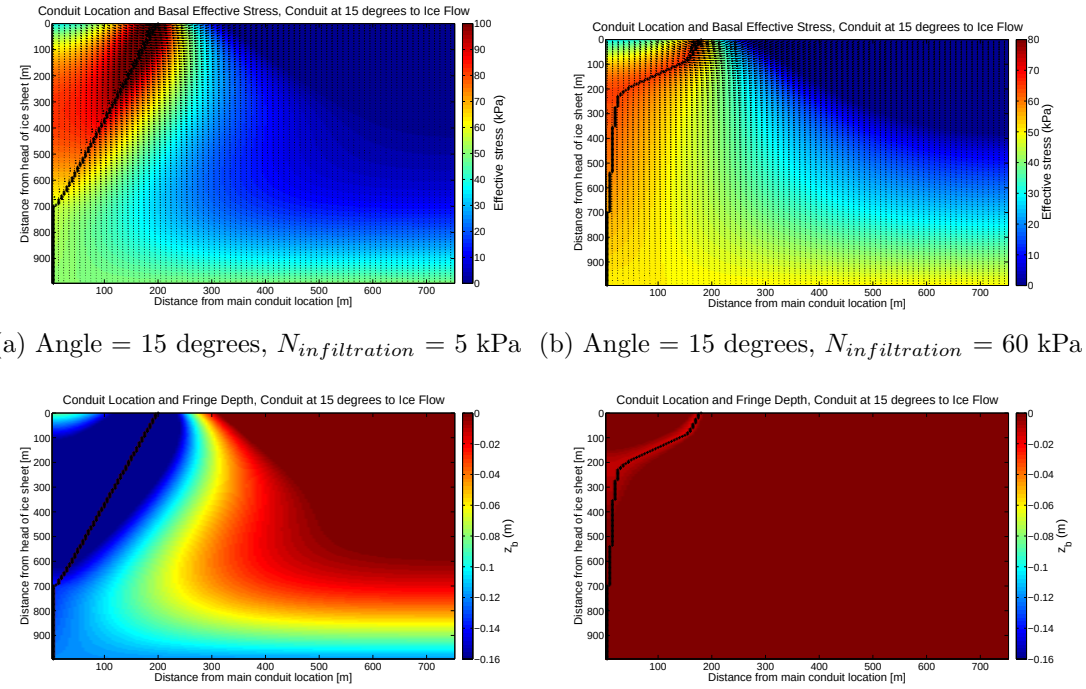

(a) Angle = 15 degrees, $N_{infiltration}$ = 5 kPa (b) Angle = 15 degrees, $N_{infiltration}$ = 60 kPa

(c) Angle = 15 degrees, $N_{infiltration}$ = 5 kPa (d) Angle = 15 degrees, $N_{infiltration}$ = 60 kPa

FIGURE 10. Graph of the effective stress and ice-infiltration depths in the drainage basin where the conduit uses the effective stress and ice infiltration data generated at a set angle of 15 degrees as initial conditions. We show here the results for $N_{infiltration}$ = 5 kPa (a,b) and for $N_{infiltration}$ = 60 kPa (c,d). The conduit is indicated as a black cross and the direction of porous media flow is indicated by the vector field.

based on assumptions of an ice surface sloping steadily in the y-direction. These assumptions favor the supression of branching in that the dominant influence of the surface slope in determining the total potential gradient is aligned only in the y-direction, whereas various surface features would locally alter these potential gradients and the path of water flow. Additionally, by altering our assumption of uniform sediment characteristics (i.e. porosity, permeability, and density), local changes in the highest potential gradient may occur without requiring changes in the surface slope.

In our overall evaluation of the self-selected conduit paths, we find that ice infiltration of the till establishes obstacles to water flow, forcing networks to branch at low angles that maintain regions of high effective stress between branches and maintaining an ice fringe of sufficient depth to impair water flow across a central divide.

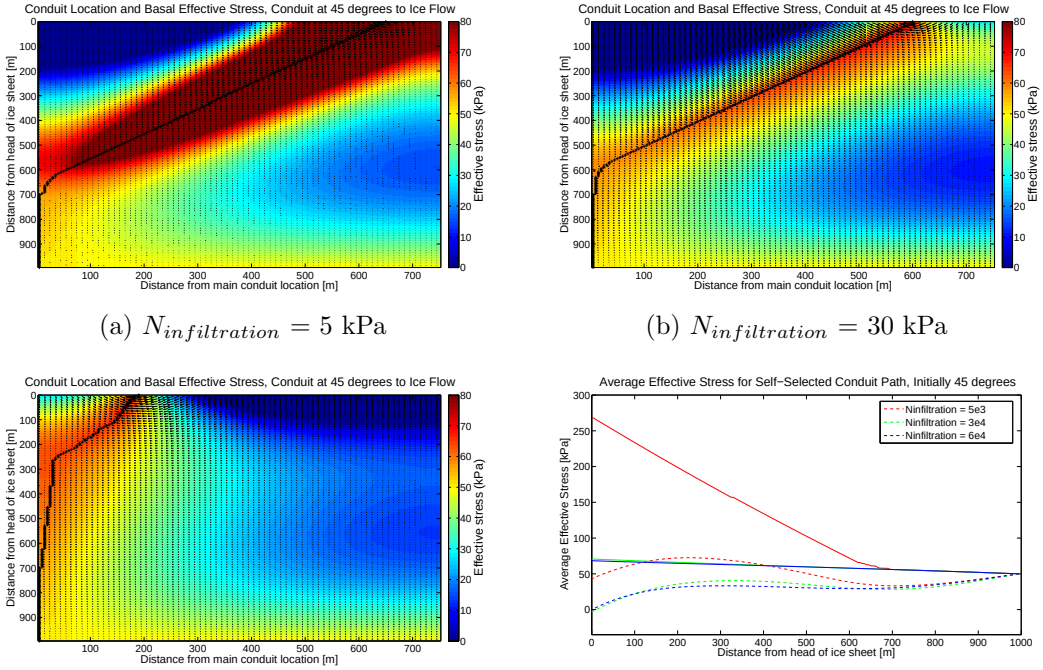

(a) $N_{infiltration} = 5$ kPa

(b) $N_{infiltration} = 30$ kPa

(c) $N_{infiltration} = 60$ kPa

(d) Angle = 15 degrees

FIGURE 11. Graphs of the effective stress in the drainage basin after the conduit has selected its path after setting the initial conduit path to 45° are shown for $N_{infiltration} = 5$ (a), 30 (b), and 60 kPa (c). The conduit is indicated as a black cross and the direction of porous media flow is indicated by the vector field. For comparison, we show the conduit effective stress (solid) and average effective stress in the surrounding bed (dashed) for these scenarios (d), where $N_{infiltration} = 5$, 30, and 60 kPa are indicated by red, green, and blue lines respectively.

Infiltration of ice into the till in these regions may contribute additional resistance to the flow of the overlying ice, inducing regions of slower sliding surrounded by faster regions, 'sticky-spots.' This type of feature is identifiable

in ice surface velocity measurements and may serve to locate areas where water pressure is relatively low, allowing us to assess the structure of the local hydrologic network. It is also important to note that differences in the change in effective stress over the length of the conduit for each of the pre-set angles (Figure 8) is small relative to the background effective stress, though the bed effective stress varies significantly for each geometry. From this observation, we conclude that measurements of effective stress and volumetric flux within the conduit while useful for informing models like these, do not necessarily indicate a specific network geometry.

In establishing conduit networks beneath an ice sheet, however, it may be difficult for ice to infiltrate the till quickly enough to establish the conditions we have identified for potentially viable network configurations. Work by Rempel (2009) indicates that the time scale of ice infiltration is limited by the need to conduct away latent heat and can range between between 11 and 2,000 years under typical conditions. Since ice flow over a steady-state drainage network will expose a given parcel of basal ice to changing levels of effective stres, the infiltration of ice into till that we envision here has transient aspects. Our simplified treatment with transmissivity as a linear function of the local effective stress is intended as a first step toward accounting for the dynamic equilibrium that may result. Additionally, the establishment of a conduit network may be inhibited by an increase in basal frictional heating causing increased melting due to the increased roughness caused by incorporation of till into the basal ice. The presence of additional water may sufficiently overwhelm the system such that rapid sliding occurs, destroying the developing conduit network.

CHAPTER V

CONCLUSION

In this study, we evaluate various network geometries for conduits cut into porous media in order to determine whether they are likely to exist beneath an ice sheet given conditions typical to those of the East Antarctic Ice Sheet. We use an ODE solver to determine the effective stress and volumetric flux in these conduits and a finite difference model to evaluate the effective stress in the surrounding bed. Given these model pieces, we determine the steady-state configuration of the networks forced to branch at specified angles. We further assess these steady-state systems by calculating the highest gradient in hydraulic potential for a conduit system using an ODE solver in order to determine if conduit flow would occur at the originally imposed geometry. We solve our governing equations for porous media flow using a finite difference method and allowing ice infiltration of the pore space to occur at a critical effective stress $N_{infiltration}$ that we vary within network geometries. We find that for low values of $N_{infiltration}$, ice infiltration of sediment allows conduits initiated at specified angles to follow the paths originally imposed on these systems. Where insufficient ice infiltration occurs, the highest hydraulic potential gradient remains aligned parallel to the gradient in ice surface elevation. Our results speak to the importance of incorporating small-scale processes into models of subglacial hydrologic networks.

Given the importance of ice infiltration into subglacial till to conduit network geometry, future investigations should include variation in the transmissivity, porosity, and density of the till bed. Future work might also

consider the increase in basal friction caused by incorporation of till into the base of the glacier. Alternative studies might investigate the affect of imposing a nonuniform surface gradient in order to cause the highest gradient in hydraulic potential to vary without the incorporation of small-scale processes in till bedded-regions or in hard-bedded regions.

APPENDIX A

CALCULATION OF BASAL MELT RATE

In order to determine the amount of heat available for conversion of ice to water through melting at the base of an ice sheet, we consider three local heat fluxes. We use intermediate values of the parameters required to calculate the melt rate, where ranges are summarized in Appendix 2. Geothermal heat conducted up through the rock at the base of the ice sheet provides a local heat flux Q_g. Estimates of this flux have been inferred as $Q_g \approx 0.05 \pm 0.02$ W/m^2 (Shapiro and Ritzwoller, 2004). Sliding at the base of the ice sheet also produces heat, which can be calculated by multiplying the basal shear stress and the sliding rate. Over inland areas of the East Antarctic Ice Sheet, we see a sliding rate of $W_s \approx 20 \pm 10$ m/yr (Rignot et al., 2011). Using the BEDMAP dataset (BAS, 2000)[1], we calculate the basal shear stress τ_b in these locations using the ice thickness H and surface slope ∇z_s such that

$$\tau_b = \rho_i \cdot g \cdot H \cdot \nabla z_s. \tag{A.1}$$

We estimate τ_b as 40 ± 10 kPa, consistent with values reported by Joughin et al. (2006) for the fringes of ice stream Recovery B, which extend into the Recovery Basin, a basin in the East Antarctic Ice Sheet whose sliding rate and geothermal heat flux motivate our choice of parameters for this study. The local

[1]British Antarctic Survey

heat flux from frictional sliding and basal ice deformation is

$$Q_f = \tau_b \cdot W_s = (40 \times 10^3 \text{ Pa}) \cdot (20 \text{ m/yr}) \approx 0.03 \text{ W/m}^2. \tag{A.2}$$

Heat is also lost at the bed as it is conducted away from the bed-ice interface. The difference in temperature between the bed (0 ^{o}C) and the surface ($\approx$ -40 $\pm$ 3 ^{o}C) (Comiso, 2000) determines the thermal gradient over the thickness of the ice ($\approx$ 2500 m from BAS (2000)). The local heat flux away from the bed Q_b can therefore be estimated by multiplying the thermal gradient at the bed and the thermal conductivity of ice such that

$$Q_b = k_{ice} \cdot \frac{\Delta \mathcal{T}}{H} = 2.2 \text{ W/(m } \cdot^o\text{C)} \left(\frac{-40 \ ^o\text{C}}{2500 \text{ m}} \right) \approx -0.03 \text{ W/m}^2. \tag{A.3}$$

This calculation of basal heat flux provides a first blush estimate of the processes at work. Additional processes that affect this heat flux include advection of heat by ice flow, which might introduce additional heat to the system and energy dissipation by ice deformation, which would reduce our estimate.

In order to determine the rate at which basal melting occurs, we equate the heat available for meltwater production Q_{melt} with the local heat fluxes such that

$$Q_{melt} = Q_f + Q_g + Q_b \approx 0.05 \text{ W/m}^2. \tag{A.4}$$

If we assume that all of the heat available for melting produces melt at a rate $\dot{m}$, then the local heat flux can be related to the total water mass produced

by melting per time multiplied by the latent heat of fusion L to determine this rate of melting

$$Q_{melt} = \rho_i \cdot \dot{m} \cdot L = Q_f + Q_g + Q_b \tag{A.5}$$

$$\dot{m} = \frac{(Q_f + Q_g + Q_b)}{\rho_i \cdot L} \approx \frac{(0.05 \text{ W/m}^2)}{920 \text{ kg/m}^3 \cdot 3.35 \times 10^5 \text{ J/kg}} \tag{A.6}$$

$$\dot{m} \approx 5 \pm 3 \text{ mm/yr.} \tag{A.7}$$

The heat balance implies that meltwater is generated beneath the ice sheet at a rate of approximately 5 mm/yr. Our model describes how this water makes its way out from underneath the ice sheet by both conduit flow and porous media flow. We assume that the only local influx of water into our system is provided by basal melting, and thus this melting rate results in a relatively 'dry' bed when compared with ice sheets experiencing the additional input of surface melting, high geothermal heat flux, or faster sliding rates.

APPENDIX B

DERIVATION OF GOVERNING EQUATIONS FOR POROUS MEDIA FLOW

In this model we consider that the overlying ice sheet sits on a 0.1 - 10 m bed of uniform thickness till (Walder, 1982) that itself sits on impermeable bedrock. Meltwater generated at the top of the till layer migrates toward conduits carved into the till. These conduits rely on a steady influx of water from the surrounding bed Ω. We assume that this till layer is entirely saturated with water and that if water cannot migrate to the channel, water pressure builds such that the effective stress far from the conduit becomes zero and the overlying ice sheet experiences flotation. Should flotation occur, a new conduit may be required to transport additional water from the saturated till. We do not address this complication, but focus instead on the evacuation of meltwater from beneath the ice sheet for a steady-state subglacial hydrologic network.

In order to determine the contribution of water from the till to the conduit, we set up our model such that conduits flow through a bed of till that is characterized by Darcy flow. Boundary conditions for a finite difference model are required at hydrologic divides. Given the branching nature of our conduit system, the divides parallel to the conduit are therefore located between adjoining branches and between conduit networks at the limit of a given network's influence where water does not flow across these boundaries. The uppermost boundary represents the transition from areas where porous media flow still serves to evacuate all meltwater to the region in which sufficient water gathers to carve out a conduit to better drain the till. The lower boundary

of our model remains at constant effective stress and is perpendicular to the conduit, indicating that our model terminates in either a change of transport mechanism or a site of water storage, like a subglacial lake.

In order to incorporate the physical process of melt migration through till, we consider that water migrates from areas of high pressure to areas of low pressure. We first define the hydrostatic P_{hydro} and nonhydrostatic δP components of water pressure beneath the ice-bed interface at z_o so that

$$\begin{aligned} P_{hydro}(z) &= P(z_b) + \rho_w g(z_b - z), \\ \text{and } P(z) &= P_{hydro}(z) + \delta P(z) \\ &= P(z_b) + \rho_w g(z_b - z) + \delta P(z), \end{aligned} \tag{B.1}$$

where g is the acceleration of gravity, ρ_w is the water density, and the upper boundary of water-saturated till is located at z_b, which we will allow to vary as ice infiltration occurs. By substituting this definition of pressure into Darcy's Law, we obtain an equation for water velocity $\vec{u}$ through till with permeability k in three dimensions and simplify the equation such that

$$\begin{aligned} \vec{u} &= \frac{-k}{\mu} \nabla \left[P(z_b) + \rho_w g(z_b - z) + \rho_w g z + \delta P(z) \right] \\ \vec{u} &= \frac{-k}{\mu} \nabla \left[P(z_b) + \rho_w g z_b + \delta P(z) \right], \end{aligned} \tag{B.2}$$

where μ is the water viscosity.

We calculate the depth-averaged flow rate $\overline{u}$ as

$$\overline{u} = \frac{1}{b} \int_0^b \frac{-k}{\mu} \nabla \left[P(z_b) + \rho_w g z_b + \delta P(x, y, z) \right] dz,$$

where b is the thickness of the water-saturated zone. We integrate all but the non-hydrostatic component of pressure while assuming that permeability k and water viscosity μ are constant such that

$$\overline{u} = \frac{1}{b}\frac{-k}{\mu}\left[\nabla\left(P(z_b)+\rho_w g z_b\right) b + \int_0^b \nabla\left(\delta P\right) dz\right] \tag{B.3}$$

$$\overline{u} = \frac{-k}{\mu}\nabla\left(P(z_b)+\rho_w g z_b\right)\left[1+\frac{1}{b}\frac{1}{\nabla\left(P(z_b)+\rho_w g z_b\right)}\int_0^b \nabla\left(\delta P\right) dz\right]. \tag{B.4}$$

We focus on cases where the contribution of non-hydrostatic gradients is small so that

$$\begin{aligned}\overline{u} &= \frac{-k}{\mu}\left[1+\frac{1}{b}\frac{1}{\nabla\left(P(z_b)+\rho_w g z_b\right)}\int_0^b \nabla\left(\delta P\right) dz\right]_{small}\nabla\left(P(z_b)+\rho_w g z_b\right)\\ &= \frac{-k}{\mu}\nabla\left(P(z_b)+\rho_w g z_b\right).\end{aligned} \tag{B.5}$$

Having solved for the depth-averaged flow rate, we rewrite water pressure in terms of the overburden pressure σ and the effective stress N at $z_b < 0$, where ϕ is porosity and ρ_t is the density of the till,

$$P(b) = \sigma - N \tag{B.6}$$

$$= \rho_i g\left(z_s - \phi z_b\right) - (1-\phi)\rho_t g z_b - N, \tag{B.7}$$

$$\text{and } \overline{u} = \frac{-k}{\mu}\left(\rho_i g\nabla(z_s-\phi z_b) - (1-\phi)\rho_t g\nabla z_b - \nabla N + \rho_w g\nabla z_b\right). \tag{B.8}$$

As a result of our integration, we find that the average flow velocity does not require knowledge of the thickness of the till through which water flows,

only knowlege of the gradients driving flow, the permeability of the sediment, and the water viscosity. Melt from the base of the ice sheet is supplied at the rate calculated by the heat balance (A.7) and causes a divergence in the water flux through the till so that

$$\nabla \cdot (\overline{u}b) = \dot{m} \; . \tag{B.9}$$

We calculate the effective stress at the base of the ice sheet by accounting for this source of water and the gradient in gravitational potential energy caused by the weight of the overlying material where ice-saturated till has a density $\rho_b = \phi\rho_i + (1-\phi)\rho_t$,

$$\psi = -\rho_i g \nabla z_s - (\rho_w - \rho_b) g \nabla z_b, \tag{B.10}$$

which is controlled by gradients in the glacier surface height ∇z_s and in the elevation of the basal interface with water-saturated till ∇z_b. In the absence of ice-infiltration of till, changes in the surface elevation dominate the potental gradient as the density contrast between water and ice dampens the effect of changes in bed surface elevation. Due to ice infiltration of till, where $\rho_b \approx 2\rho_w$, changes in the bed surface elevation contribute approximately equally to the potential gradient. Combining (B.8), (B.9) and (B.10) gives the melt rate as

$$\begin{aligned} \dot{m} &= \nabla \cdot \left(\frac{bk}{\mu} \left[\psi + \nabla N \right] \right) \\ \text{when } \mid \dot{m} \mid &<< \left| \frac{k}{\mu} \nabla \left(P(z_b) + \rho_w g z_b \right) \right| . \end{aligned} \tag{B.11}$$

The thickness of till through which water flows b regulates the local transmissivity

$$T = b \cdot K_{sed}, \tag{B.12}$$

where the hydraulic conductivity K_{sed} and permeability are related by $\rho_w g k = \mu K_{sed}$. At a critical effective stress $N_{infiltration}$, ice begins to infiltrate the till (Rempel, 2009), reducing b and thus reducing T. Recognizing the dependence of transmissivity on effective stress, we approximate the decrease in transmissivity with effective stress by

$$\begin{aligned} T &= T_o \text{ for } N \leq N_{infiltration} && \text{(B.13)} \\ \text{and } T &= T_o + \lambda(N - N_{infiltration}) \text{ for } N > N_{infiltration}. && \text{(B.14)} \end{aligned}$$

where T_o is the transmissivity before ice is able to infiltrate the till and λ is treated as a positive constant for simplicity. Substituting into the relationship between meltwater input and Darcy flow (B.11) gives

$$\begin{aligned} \dot{m}\, \rho_w g &= \nabla \cdot [T\psi] + \nabla \cdot [T \nabla N] && \text{(B.15)} \\ \dot{m}\, \rho_w g &= (\nabla T) \cdot \psi + T\,(\nabla \cdot \psi) + (\nabla T) \cdot \nabla N + T\left(\nabla^2 N\right). && \text{(B.16)} \end{aligned}$$

Using the relationship between gradient in transmissivity and gradient in effective stress, this equation further simplifies to

$$\nabla^2 N = \frac{\dot{m}\, \rho_w g}{T} - \nabla \cdot \psi - \frac{\lambda}{T} \nabla N \cdot \psi - \frac{\lambda}{T} (\nabla N)^2 \tag{B.17}$$

where we note that $\lambda = 0$ when $N \leq N_{infiltration}$.

Our governing equation (B.17) reflects the dependence of the change in effective stress on the melt rate, transmissivity, and geometry of the ice sheet. In our model, we assume that the height of the ice sheet surface varies only in the y-direction as

$$z_s = H + S_s y \tag{B.18}$$

where the surface slope is S_s and change in the ice surface height is constant in $\widehat{x}$. Due to the assumed constant surface slope, the gradient in ψ that contributes to changes in the water transport rate (B.17) is dependent only on variations in z_b.

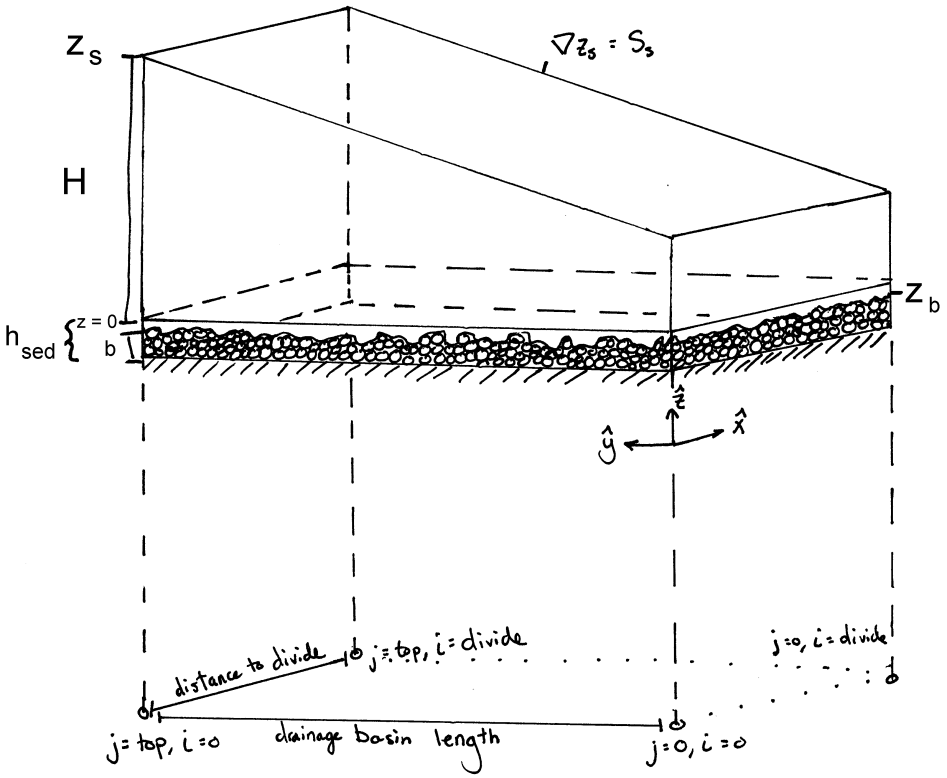

FIGURE 12. Rough diagram showing parameter definitions as well as how the finite difference model relates to the physical boundaries of the system.

To solve our field equation for distribution of effective stress along the glacier base (B.17), we must first specify conditions along the boundaries of the model domain. We expect that no water flows across the hydrologic divides at $x = 0$ and $x = x_{\max}$ such that

$$\overline{u}_x(divide) = 0, \tag{B.19}$$

Since there are no changes in z_s or z_b across the hydrologic divides, (B.8) implies that the x-components of the gradients in effective stress vanish such that $\partial N/\partial x = 0$ at $x = 0$ and $x = x_{\max}$, providing a boundary condition for our finite difference model at these locations. At the lower boundary, we assume a constant effective stress consistent with the effective stress at the outlet of the conduit, indicating that our model terminates in either a change of transport mechanism or a site of water storage like a subglacial lake. Across the upper boundary, we specify a constant Darcy flow rate as might be contributed from a collection area located beyond the reach of a channelized system. Using (B.8) to solve for effective stress gradient resulting from this boundary condition such that

$$\begin{aligned} b\overline{u} \cdot \widehat{y} = c_t &= \frac{T}{\rho_w g}\left(-\rho_i g \nabla z_s + \nabla N - (\rho_w - \rho_b) g \nabla z_b\right) \cdot \widehat{y} \\ \frac{c_t \rho_w g}{T} &= -\rho_i g S_s - (\rho_w - \rho_b) g \frac{\partial z_b}{\partial y} + \left.\frac{\partial N}{\partial y}\right|_{y=top}. \end{aligned}$$

By recalling that basal elevation is defined as the height of infiltration into the till from the base of the ice sheet where $b = z_b + h_{sed}$, we define the change in z_b across this boundary as a function of the change in effective stress (B.14) in the same direction. We then solve for the gradient in effective stress across the

upper boundary of the model such that

$$\begin{aligned} \frac{c_t \rho_w g}{T} + \rho_i g S_s &= (1 - (\rho_w - \rho_b) g \lambda / K_{sed}) \left. \frac{\partial N}{\partial y} \right|_{y=top} \\ \left. \frac{\partial N}{\partial y} \right|_{y=top} &= \frac{\frac{c_t \rho_w g}{T} + \rho_i g S_s}{1 - (\rho_w - \rho_b) g \lambda / K_{sed}}. \end{aligned} \tag{B.20}$$

Finite Difference Formulation

In our coordinate system, the 'top' of the finite difference model, where $y(top)$ is equal to the length of the entire drainage basin considered divided by the number of nodes. The coordinate system and boundary conditions used in the model assume that branching occurs symmetrically around a central conduit that is supplied by meltwater from both sides of the conduit and whose subsequent branches are supplied only by meltwater from between the central and far hydrologic divide. When we discuss the field equations in terms of a finite difference equation, we will discuss the effect of these boundary conditions on the field equations. Written in terms of partial derivatives with respect to the x- and y- coordinates, the field equation becomes

$$\begin{aligned} \frac{\partial^2 N}{\partial x^2} + \frac{\partial^2 N}{\partial y^2} &= \frac{\dot{m}\, \rho_w g}{T} - \left(\frac{\partial \psi}{\partial x} + \frac{\partial \psi}{\partial y} \right) \\ &- \frac{\lambda}{T} \left(\frac{\partial N}{\partial x} \psi_x + \frac{\partial N}{\partial y} \psi_y \right) - \frac{\lambda}{T} \left[\left(\frac{\partial N}{\partial x} \right)^2 + \left(\frac{\partial N}{\partial y} \right)^2 \right] \\ \frac{\partial^2 N}{\partial x^2} + \frac{\partial^2 N}{\partial y^2} &= \frac{\dot{m}\, \rho_w g}{T} + (\rho_w - \rho_b) g \left(\frac{\partial^2 z_b}{\partial x^2} + \frac{\partial^2 z_b}{\partial y^2} \right) + \frac{\lambda (\rho_w - \rho_b) g}{T} \left(\frac{\partial N}{\partial x} \frac{\partial z_b}{\partial x} \right) \\ &+ \frac{\lambda}{T} \left(\frac{\partial N}{\partial y} \right) \left(\rho_i g \frac{\partial z_s}{\partial y} + (\rho_w - \rho_b) g \frac{\partial z_b}{\partial y} \right) - \frac{\lambda}{T} \left[\left(\frac{\partial N}{\partial x} \right)^2 + \left(\frac{\partial N}{\partial y} \right)^2 \right] \end{aligned}$$

For a second order difference of a function f over a distance h,

$$f''(x) = \frac{f(x+1) - 2f(x) + f(x-1)}{h^2}, \tag{B.21}$$

and when we apply this equation to our governing equation for a uniform grid spacing ($dy = dx$), we can solve for the effective stress in a location in terms of the nodes around it using a 5-point stencil where N is the effective stress at a node, positive j indicates the upstream y-direction, and positive i indicates the x-direction such that

$$\begin{aligned} \frac{\partial^2 N}{\partial x^2} + \frac{\partial^2 N}{\partial y^2} &= \frac{N_{i+1,j} - 2N_{i,j} + N_{i-1,j}}{dx^2} + \frac{N_{i,j+1} - 2N_{i,j} + N_{i,j-1}}{dy^2} \\ &= \frac{N_{i+1,j} + N_{i-1,j} + N_{i,j+1} + N_{i,j-1} - 4N_{i,j}}{dy^2}. \end{aligned} \tag{B.22}$$

For a slope over a distance $2h$,

$$f'(x) = \frac{f(x+1) - f(x-1)}{2h} \tag{B.23}$$

and so we write the rest of the components of Eq. (B.21) out in the same manner such that

$$
\begin{aligned}
&\frac{\dot{m}\,\rho_w g}{T} = \frac{\dot{m}\,\rho_w g}{T_{i,j}} \\
&(\rho_w - \rho_b) g \left(\frac{\partial^2 z_b}{\partial x^2} + \frac{\partial^2 z_b}{\partial y^2} \right) \\
&\quad = (\rho_w - \rho_b) g \left(\frac{z_{b(i+1,j)} + z_{b(i-1,j)} + z_{b(i,j+1)} + z_{b(i,j-1)} - 4 z_{b(i,j)}}{dy^2} \right) \\
&\frac{\lambda(\rho_w - \rho_b) g}{T} \left(\frac{\partial N}{\partial x} \frac{\partial z_b}{\partial x} \right) \\
&\quad = \frac{\lambda(\rho_w - \rho_b) g}{T} \left(\frac{N_{i+1,j} - N_{i-1,j}}{2dx} \right) \left(\frac{z_{b(i+1,j)} - z_{b(i-1,j)}}{2dx} \right) \\
&\frac{\lambda}{T} \left(\frac{\partial N}{\partial y} \right) \rho_i g \frac{\partial z_s}{\partial y} \\
&\quad = \frac{\lambda}{T_{i,j}} \left(\frac{N_{i,j+1} - N_{i,j-1}}{2dy} \right) \rho_i g S_s \\
&\frac{\lambda}{T} \left(\frac{\partial N}{\partial y} \right) (\rho_w - \rho_b) g \frac{\partial z_b}{\partial y} \\
&\quad = \frac{\lambda}{T_{i,j}} \left(\frac{N_{i,j+1} - N_{i,j-1}}{2dy} \right) \left((\rho_w - \rho_b) g \frac{z_{b(i,j+1)} - z_{b(i,j-1)}}{2dy} \right) \\
&-\frac{\lambda}{T} \left[\left(\frac{\partial N}{\partial x} \right)^2 + \left(\frac{\partial N}{\partial y} \right)^2 \right] \\
&\quad = -\frac{\lambda}{T_{i,j}} \left[\left(\frac{N_{i+1,j} - N_{i-1,j}}{2dx} \right)^2 + \left(\frac{N_{i,j+1} - N_{i,j-1}}{2dy} \right)^2 \right].
\end{aligned}
$$

It is important that none of these components is dependent on $N_{i,j}$ and the field equation allows us to use an iterative solution technique to solve for

effective stress such that

$$\begin{aligned} N_{i,j} &= \frac{1}{4}\left(N_{i+1,j}+N_{i-1,j}+N_{i,j+1}+N_{i,j-1}\right)-\frac{\dot{m}\,\rho_w g\cdot dy^2}{4T_{i,j}} \\ &- \frac{(\rho_w-\rho_b)g}{4}[z_{b(i+1,j)}+z_{b(i-1,j)}+z_{b(i,j+1)}+z_{b(i,j-1)}-4z_{b(i,j)}] \\ &- \frac{\lambda(\rho_w-\rho_b)g}{16T_{i,j}}(N_{i+1,j}-N_{i-1,j})(z_{b(i+1,j)}-z_{b(i-1,j)}) \\ &- \frac{\lambda(\rho_w-\rho_b)g}{16T_{i,j}}(N_{i,j+1}-N_{i,j-1})(z_{b(i,j+1)}-z_{b(i,j-1)}) \\ &- \frac{\lambda\rho_i g\cdot dy}{8T_{i,j}}S_s(N_{i,j+1}-N_{i,j-1}) \\ &+ \frac{\lambda}{16T_{i,j}}\left[(N_{i+1,j}-N_{i-1,j})^2+(N_{i,j+1}-N_{i,j-1})^2\right]. \end{aligned} \tag{B.24}$$

Given the boundary conditions discussed previously for the hydrologic divides,

$$\left.\begin{aligned} N_{0,j} &= N_{2,j}, \text{ and} \\ z_{b(0,j)} &= z_{b(2,0)} \end{aligned}\right\} x=0$$

$$\left.\begin{aligned} N_{max-1,j} &= N_{max+1,j}, \text{ and} \\ z_{b(max-1,j)} &= z_{b(max+1,j)} \end{aligned}\right\} x=x_{\max}$$

and for the upper bound of the model

$$N_{i,j-1}=N_{i,j+1}-\frac{\frac{c_t\rho_w g}{T_{i,j}}+\rho_i g S_s}{1-(\rho_w-\rho_b)g\lambda/K_{sed}} \tag{B.25}$$

so that the values of nodes outside the extent of our model are not required. After each iteration of the finite difference model, we calculate the transmissivity of the bed at each node (B.14), and from this value determine z_b.

The final condition required by our finite difference model is the value of the effective stress in the conduit and the location of that conduit. The effective stress in the conduit for each conduit node is determined by the conduit flow model described in Appendix C. After the effective stress and the location of the conduit are determined, the coordinates of the conduit are matched to the nearest node, which then retains the effective stress at that point in the conduit. We then run the finite difference model using these conditions for the hydrologic divides, top boundary condition, constant lower bound, and conduit effective stress in conjunction with the field equation (B.24) to determine the effective stress at the ice-bed interface for each node of our model.

Given the values of effective stress and the depth of infiltration of the ice into the till, we calculate the magnitude and direction of flow

$$\overline{u} = \frac{-k}{\mu} \left(\rho_i g \nabla z_s - \nabla N + (\rho_w - \rho_i) g \nabla z_b \right). \tag{B.26}$$

Sucessive integrations of the conduit flow model are then informed by the information gained through this porous media flow model, where the supply of melt to a given section of conduit per meter of conduit Ω is defined as the component of melt perpendicular to the conduit

$$\Omega = |\overline{u}| b sin(\theta) \tag{B.27}$$

where the angle θ is defined on the diagram in Figure 13 and Ω represents the volume of water supplied to the conduit when integrated over the the conduit segment of length ℓ. We perform this process of determining the melt supply to the conduit for the nodes supplying the conduit on either side of the proposed

conduit segment, where the central conduit is supplied by melt from either side of the y-axis keeping in mind the assumption of symmetrical branching.

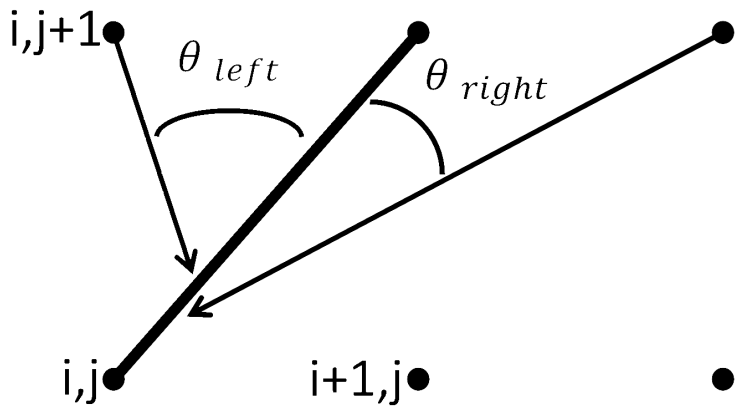

FIGURE 13. Visual representation of the calculated water flow. The solid path represents the section of conduit supplied by these adjacent nodes, where the arrows indicate the direction of water flow (B.26). These arrows are plotted on a map of effective stress following the completion of the model.

APPENDIX C

DERIVATION OF CHANNELIZED FLOW EQUATIONS

In Nye's 1976 discussion of water flow in glaciers, he derived a generalized set of equations for water flow in a conduit. This derivation is based on previous work by Rothlisberger (1972) and Weertman (1972). I present his derivation here and state the assumptions that allow further simplification of these equations to the form used in my model. These equations are derived for a conduit that is filled with water. To fully describe the processes in a conduit thermodynamically we must consider the work associated with the change of conduit diameter, the dependence of melting point on pressure, and the temperature gradient along the tunnel.

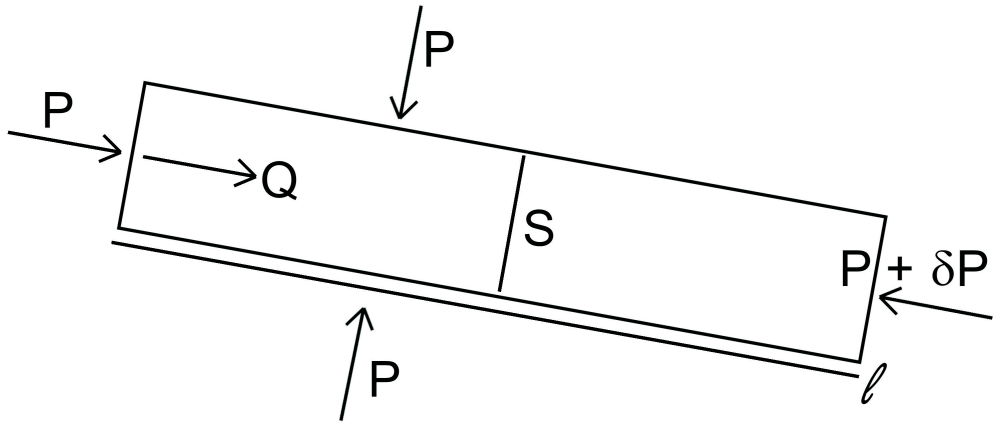

FIGURE 14. Visual representation of the conduit system. We assume that this segment of the conduit is short and that the length ℓ is a function of both time and location.

We first consider the processes affecting a given cross-section of conduit. The conduit experiences turbulent water flow, causing frictional heating and

melting but it is simultaneously contracting due to plastic deformation of the ice around it. Changes in these processes are reflected in changes in the cross-sectional area S of the conduit section over time as

$$\frac{\partial S}{\partial t} = \underbrace{\frac{M}{\rho_i}}_{\text{melt contribution}} + \underbrace{\left(\frac{\partial S}{\partial t}\right)_{plastic}}_{\text{plastic contribution}} \tag{C.1}$$

where M is the melting rate of the conduit walls and a nonlinear ice rheology is most appropriate for plastic ice flow. Based on research by Glen (1955), the creep of ice in a conduit with a circular cross-section is proportional to the effective stress in the conduit N_c raised to a creep exponent, which he experimentally determined to be approximately three. This deformation is also proportional to a constant, K_0, much like viscosity in that it is a material property. In the case of ice, this constant is dependent on both temperature and fabric and for simplicity, we implement a linear ice rheology such that $n = 1$. The plastic deformation of a conduit cross-section is

$$\left(\frac{\partial S}{\partial t}\right)_{plastic} = -K_0 S N_c^n. \tag{C.2}$$

We assume that the change in water mass in this system is only a function of $\frac{\partial S}{\partial t}$ and the change in volume flux of water across the cross-section $\frac{\partial Q}{\partial s}$, where these changes are partly balanced by the water contribution from the melting conduit walls. Nye (1976)'s formulation for continuity does not include the contribution of water from the bed Ω, though we include it here as an additional

source of water such that

$$\frac{\partial Q}{\partial s} + \frac{\partial S}{\partial t} = \frac{M}{\rho_w} + \Omega. \tag{C.3}$$

By the first law of thermodynamics, since there are no kinetic energy inputs, we can equate the total change in energy of the system to the rate of work done on the system. Work is done on this system by the external pressure, which causes contraction of the conduit, by the water pressure on both the upstream and downstream boundaries and by gravity. The external pressure pushes in on the system in order to cause plastic deformation and is resisted by the internal water pressure P. This water pressure also does work on the system at the upstream and downstream ends of the conduit section, over which a change in both the conduit pressure and the volumetric flow rate occurs within the conduit. Lastly, the downstream-component of gravity g_s does work on the system by acting on the water mass flowing through the conduit section.

If we assume that the water is well-mixed by turbulent flow, then the change in internal energy is due to the change in temperature of the water over time and the difference between the temperature of the water flowing in the conduit and the temperature of a thin film of water at the melting temperature present at the ice-water interface. To determine the amount of energy required to raise the water temperature in the conduit of mass $S\ell\rho_w$, we multiply the specific heat C and the rate of temperature change. The total amount of energy required to both melt water and incorporate it into the system is a function of both the difference in internal energy between the water and ice $\Delta u = L - P\Delta v$ and the amount of energy required to raise the temperature of the water in film Θ_i to the temperature of water in the conduit Θ_w. The change in internal

energy that occurs as a result of melting is equal to the difference between the latent heat of melting and the pressure of the system multiplied by the volume change. By assuming an isothermal system, we find that the change in internal energy per length of conduit is

$$\underbrace{\cancel{-P\left(\frac{\partial S}{\partial t}\right)_{plastic}}}_{\substack{\text{work done on system}\\ \text{by pressure causing}\\ \text{plastic deformation}}} - \underbrace{\frac{\partial (PQ)}{\partial s}}_{\substack{\text{work done on}\\ \text{system by water}\\ \text{pressure on upstream}\\ \text{and downstream}\\ \text{boundaries}}} + \underbrace{Q\rho_w g_s}_{\substack{\text{work done by gravity}}}$$

$$= \underbrace{\cancel{S\rho_w C\frac{d\Theta_w}{dt}}\delta t}_{\substack{\text{internal energy}\\ \text{needed to raise}\\ \text{the temperature}\\ \text{of conduit water to}\\ \Theta_w}} + \underbrace{M[L - \cancel{P\Delta v} + \cancel{C(\Theta_w - \Theta_i)}]}_{\substack{\text{internal energy}\\ \text{needed to generate}\\ \text{new melt and raise}\\ \text{melt to temperature}\\ \text{of conduit}}}, \quad \text{(C.4)}$$

where the plastic deformation term is canceled by the change in internal energy due to a change in volume. If we assume that the volumetric flow that does work at the ends of the conduit section is constant and that the cross-sectional area and length are both constant as well, we can rewrite this equation to isolate the heat output used in melting from the other terms leaving only

$$Q(\rho_w g_s - \frac{\partial P}{\partial s}) = ML. \quad \text{(C.5)}$$

We have thus related the pressure gradient to the volumetric flow along the conduit using a thermodynamic approach, but we can also relate these variables by considering the relationship between the mean velocity for turbulent flow and the heat generated by friction by this flow through a rough

conduit. The mean velocity $\overline{u}$ is the flow rate per area and is a function of the pressure gradient, where these quantities can be related by the Gauckler-Manning formula, which has been used by Rothlisberger (1972) for subglacial conduits. This formulation considers the hydraulic radius R and Manning's roughness coefficient n' in order to take into account the shape and the effects of friction on the flow respectively. The Gauckler-Manning formula for mean velocity,

$$\overline{u} = \frac{Q}{S} = \frac{R^{2/3}}{n'} \left[\frac{1}{\rho_w g} \left(\rho_w g_s - \frac{\partial P}{\partial s} \right) \right]^{1/2}, \tag{C.6}$$

can be manipulated by defining a constant F such that

$$F = \left(\frac{S}{R^2} \right)^{2/3} \rho_w g (n')^2 \tag{C.7}$$

in order to rewrite the original formula as

$$\frac{Q^2}{S^{8/3}} F = \rho_w g_s - \frac{\partial P}{\partial s}. \tag{C.8}$$

The relationship between hydraulic radius and the cross-sectional area is such that

$$\begin{aligned} R &= \frac{S}{(perimeter)} \\ \frac{S}{R^2} &= \frac{\cancel{S}(perimeter)^2}{\cancel{S}^{\cancel{2}}} \\ &= \frac{(perimeter)^2}{S}. \end{aligned}$$

For example, in the case of semicircular conduit cross-section,

$$\begin{aligned} \frac{S}{R^2} &= \frac{(\pi r + 2r)^2}{\frac{1}{2}\pi r^2} \\ &= \frac{2(\pi + 2)^2}{\pi} \end{aligned}$$

and by using a Manning's roughness coefficient value of $n' = 0.1\ \mathrm{m}^{-1/3}/\mathrm{s}$, the constant F has a value of $\approx 650\ \mathrm{kg/m}^{-8/3}$. By rewriting the equation for mean velocity (C.8), we have compressed the geometry and friction factors into F, which does not depend on the size of the conduit and instead only depends on the shape of the conduit which we assume to be constant throughout the conduit network. In total, we now have 4 equations to describe flow of water within a conduit which can be simplified to give the governing equations for our channelized flow model. Under the assumption of a linear ice rheology $K_0 = \frac{1}{\eta_i}$, where η_i is the ice viscosity, our equation (C.1) governing the geometry and flow of ice can be written in terms of the effective stress in the conduit N_c as

$$\frac{\partial S}{\partial t} = \frac{M}{\rho_i} - \frac{S N_c}{\eta_i}. \tag{C.9}$$

The conservation of water mass is described by our continuity equations (C.3), which accounts for water input through the melting of the conduit walls as well the contribution of melt from the surrounding bed. The turbulent flow of water within the conduit is governed by the rearranged Gauckler–Manning equation (C.8) and can be rewriten in terms of the change in effective stress along the conduit as well as the potential gradient resulting from the effect of

gravity on the overlying ice ψ (B.10)

$$\frac{Q^2}{S^{8/3}}F = \psi \cdot \widehat{s} + \frac{\partial N_c}{\partial s}. \tag{C.10}$$

The energy balance within the conduit, derived earlier in terms of separate gravity and water pressure terms, can be rewritten in terms of the same geometry factor and the effective stress. As previously stated, we also assume that there is no change in temperature either along the conduit or in time, reducing our energy equation to

$$ML = Q(\psi \cdot \widehat{s} + \frac{\partial N_c}{\partial s}). \tag{C.11}$$

By assuming that the conduit is in a steady-state configuration, we take the cross-sectional area of the channel as constant in time such that $\frac{\partial S}{\partial t} = 0$. We can then solve the kinematic condition for the conduit walls (C.9) for M such that

$$\begin{aligned} 0 &= \frac{M}{\rho_i} - \frac{SN_c}{\eta_i} \\ M &= \frac{SN_c\rho_i}{\eta_i}. \end{aligned} \tag{C.12}$$

By then combining the turbulent flow law (C.10) and energy balance (C.11), we solve for cross-sectional area and substitute in our previous definition

of conduit wall melting rate M (C.12) such that

$$\begin{aligned} \frac{FQ^2}{S^{8/3}} &= \left(\psi + \frac{\partial N_c}{\partial s}\right) = \frac{ML}{Q} \\ S &= \left(\frac{FQ^3}{ML}\right)^{3/8} \\ &= \left(\frac{FQ^3\eta_i}{LN_c\rho_i}\right)^{3/11} \end{aligned} \tag{C.13}$$

and S can now be substituted into M in order to eliminate S from calculations.

$$\begin{aligned} M &= \frac{SN_c\rho_i}{\eta_i} \\ &= \frac{N_c\rho_i}{\eta_i}\left(\frac{FQ^3\eta_i}{LN_c\rho_i}\right)^{3/11} \\ &= \left(\frac{F}{L}\right)^{3/11}\left(\frac{N_c\rho_i}{\eta_i}\right)^{8/11} Q^{9/11} \end{aligned} \tag{C.14}$$

This substitution renders specific knowledge of the conduit size unnecessary and thereby reduces the potential for error introduced by estimating conduit cross-sectional area. By substituting our equation for channel melt rate (C.14), into the conservation of mass equation (C.3) and into the energy balance (C.11), we can produce two ordinary differential equations that may then be solved for in MATLAB.

$$\begin{aligned}
\frac{\partial Q}{\partial s} &= \frac{M}{\rho_w} + \Omega \\
&= \left(\frac{F}{L}\right)^{3/11} \left(\frac{N_c \rho_i}{\eta_i}\right)^{8/11} \left(\frac{Q^{9/11}}{\rho_w}\right) + \Omega \qquad \text{(C.15)} \\
\frac{\partial N_c}{\partial s} &= \frac{ML}{Q} - \psi \\
&= \left(\frac{\rho_i N_c}{\eta_i}\right)^{8/11} \left(\frac{F}{L}\right)^{3/11} \left(\frac{Q^{9/11}}{Q}\right) L - \psi \\
&= \left(\frac{F^{3/11}}{Q^{2/11}}\right) \left(\frac{N_c \rho_i L}{\eta_i}\right)^{8/11} - \psi \qquad \text{(C.16)}
\end{aligned}$$

The parameters ψ and Ω can be taken from the glacier geometry and estimates from our porous media flow model respectively. From (C.10), we know that the magnitude of the hydraulic gradient is $\nabla\Phi = \psi + \partial N_c/\partial s$. In order to determine the optimum path of the conduit, we calculate this hydraulic gradient over the length of the conduit ℓ

$$\nabla\Phi = \left(\frac{F^{3/11}}{Q^{2/11}}\right) \left(\frac{N_c \rho_i L}{\eta_i}\right)^{8/11}. \qquad \text{(C.17)}$$

By determining the hydraulic gradient for possible channel orientations measured by angle from the y-axis, we find the highest hydraulic gradient. The first time this integration is run, we impose a specific angle of branching on the conduit system by requiring it to choose the path at the given angle. This specified angle is not used in subsequent iterations of the model, where conduit branches are divided by regions of relatively high effective stress that results in infiltration of ice into the till and in some cases establishes a physical barrier to

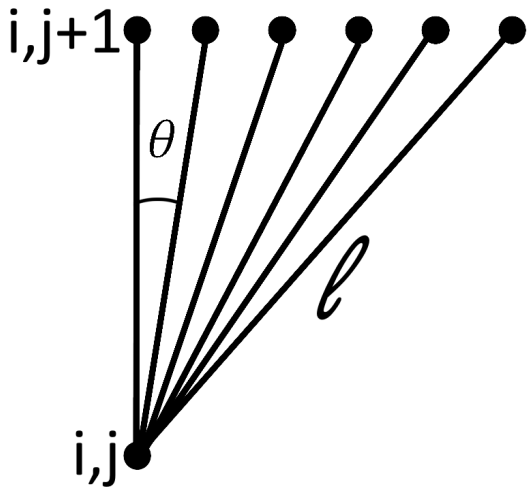

FIGURE 15. Visual representation of the various segments of conduit for which the total hydraulic gradient is calculated. We determine the ultimate path of the conduit by determining which path has the highest hydraulic gradient.

meltwater flow. This barrier may cause the highest potential gradient, which is otherwise dominated by the strong potential gradient resulting from changes in ice surface elevation, to be at an angle to the direction of ice flow.

In systems where porous media surrounds the conduit network, we see that the magnitude of change in ice penetration depth greatly influences the hydraulic gradient such that water may even flow against the gradient in the ice surface elevation. The density difference between water and ice $\rho_i g >> (\rho_w - \rho_i)g$ that allows changes in surface gradient to exert primary control on the total potential gradient in the presence of water is offset by the added weight of till incorporated into the ice such that, given full ice saturation of the pore space, $|\rho_i g| \approx |(\rho_w - \rho_i\phi - \rho_t(1-\phi))g|$. If these gradients oppose one another, Darcy flow stagnates where

$$\overline{u} = 0 = \frac{-k}{\mu}\nabla\Phi. \tag{C.18}$$

By solving for the gradient in the elevation of the ice-bed interface, we find that when

$$\nabla z_b = \frac{\nabla N - \rho_i g \nabla z_s}{(\rho_w - \rho_b)g}, \tag{C.19}$$

flow is stagnated and where ∇z_b exceeds the right-hand side value of this equation, flow can be opposite the ice surface elevation gradient. If we assume that the till is quartz, $\rho_t = 2650$ kg/m^3, and the porosity of the till is 0.35 the equation simplifies to

$$\nabla z_b = 0.88 \nabla z_s - 9.8 \cdot 10^{-5} Pa^{-1} \nabla N, \tag{C.20}$$

where assuming that the ice does not entirely saturate the pore space serves to increase the magnitude of the gradient in basal ice depth required to oppose flow. We note that the gradient in effective stress contributes relatively little to the transition in flow direction described here. For a 1 m change in z_s, ΔN would need to be on the order of 100 kPa in order to significantly influence the direction of porous media flow.

APPENDIX D

NOMENCLATURE

List of Symbols

$\Delta\mathcal{T}$	Change in temperature (^{o}C)
$\delta P(z)$	Non-hydrostatic component of water pressure at the ice-bed interface (Pa)
Δu	Difference in internal energy between the water and ice, used in derivation of channelized flow equations (J)
ℓ	Length of a short section of conduit (m)
η_i	Ice viscosity (kg/(m $\cdot$ s))
λ	Negative constant rate of ice infiltration into till (m^2/(Pa $\cdot$ s))
μ	Viscosity of water (kg/(m $\cdot$ s))
Ω	Water influx from the surrounding bed (m^2/s)
$\overline{u}$	Mean velocity of water in the conduit (m/s)
Φ	Hydraulic potential (Pa)
ϕ	Porosity of till
ψ	Potential gradient resulting from changes in the ice sheet's geometry (Pa/m)
ρ_b	Density of ice-saturated till (kg/m^3)
ρ_i	Density of ice (kg/m^3)
ρ_t	Density of till (kg/m^3)
σ	Overburden pressure resultng from weight of overlying ice sheet (Pa)
$\dot{m}$	Rate of melting at the base of the ice sheet (mm/yr)
$\vec{u}$	Water velocity through till (m/s)
τ_b	Basal shear stress (Pa)
θ	Angle between conduit and porous media flow used in calculation of Ω (degrees)
Θ_i	Temperature of water in the film, used in derivation of channelized flow equations (^{o}C)
Θ_w	Temperature of water in the conduit, used in derivation of channelized flow equations (^{o}C)
$\widehat{s}$	Downstream-direction of conduit
$\widehat{x}$	Increase in x-direction indicates icreasing distance from primary conduit
$\widehat{y}$	Positive up-glacier direction
$\widehat{z}$	Increase in the z-direction indicates increase in elevation
c_t	Constant flow rate of water

g_s	Downstream-component of gravity (m/s^2)
K_0	Constant like viscosity used to describe plastic deformation, Eq. (C.2)
k_{ice}	Thermal conductivity of ice ($W/(m \cdot {}^oC)$)
K_{sed}	Hydraulic conductivity of sediment (m/s)
n'	Manning's roughness coefficient ($s/m^{1/3}$)
P_{hydro}	Hydrostatic component of water pressure (Pa)
Q_b	Local heat flux lost from the base of the ice sheet through the overlying ice (W/m^2)
Q_f	Local heat flux generated by frictional sliding over the bed(W/m^2)
Q_g	Local heat flux from geothermal sources (W/m^2)
Q_{melt}	Energy used to generate melt at the base of the ice sheet (J)
T_o	Transmissivity of the till bed in the absence of ice infiltration (m^2/s)
W_s	Ice sheet sliding rate (m/s)
z_s	Surface height (m)
b	Thickness of till layer (m)
C	Specific heat ($J/(kg\ {}^oC)$)
dx	Spacing between nodes in x-direction (m)
dy	Spacing between nodes in y-direction (m)
F	Constant that accounts for channel shape and the manning friction coefficient, calculated as $\rho_w g n'^2 [2(\pi+2)^2/\pi]^{2/3}$ ($kg/m^{8/3}$)
H	Ice sheet thickness (m)
i	Indicates x-component of the node described
j	Indicates y-component of the node described
k	Permeability (m^2)
L	Latent heat of ice, 3.35×10^5 (J/kg)
M	Melting rate of conduit walls ($kg/(m \cdot s)$)
N	Effective stress (Pa)
n	Creep exponent
P	Water pressure (Pa)
Q	Volumetric flux (m^3/s)
R	Hydraulic radius, calculated as the cross-sectional area divided by the wetted perimeter (m)
S	Cross-sectional area of the conduit (m^2)
T	Transmissivity of sediment (m^2/s)
t	Time (s)
z	Location of the ice-bed interface (m)

APPENDIX E

NUMERICAL ALGORITHM

FOR the first iteration of the code

--prescribe a melt intake for each section of conduit

--FOR all steps in the y-direction individually

---FOR all angles

----calculate change in conduit effective stress over length of conduit using ODE45

----calculate maximum hydraulic gradient

----choose the path that deviates from the direction of ice flow by the imposed angle

----calculate the x-coordinate of the next location to integrate from

---END

--END

--Iterate until change in values between iterations below a set threshold

---FOR all points on a map of the basal effective stress (N)

----apply field equation and applicable boundary conditions

----keep the grid points that align with the conduit fixed at the value calculated previously by ODE45

---END

--END iteration

END

FOR many iterations

--FOR all steps in the y-direction individually

---FOR all angles

----calculate the amount of water drawn into the conduit by Darcy flow

----calculate change in conduit effective stress over length of conduit using ODE45

----calculate maximum hydraulic gradient

----calculate the x-coordinate of the next location to integrate from

---END

--END

--Iterate until change in values between iterations is minimal

---FOR all points on a map of the basal effective stress (N)

----apply field equation and applicable boundary conditions

---END

--END iteration

END

Parameter	**Range**	**Associated Error**	**Source**
Q_g	0.035 - 0.055 W/m^2	$\pm$0.02 W/m^2	Shapiro and Ritzwoller (2004)
W_s	7 - 30 m/yr	$\pm$ 5 - 17 m/yr	Rignot et al. (2011)
τ_b	25 - 50 kPa	$\pm$10 kPa	Joughin et al. (2006)
$\Delta\mathcal{T}$	37 - 43 ^{o}C	$\pm$3 ^{o}C	Comiso (2000)
H	2000 - 2800 m	$\pm$5 m	BAS (2000)
S_s	0.001 - 0.01 m/m	$\pm$ 0.001 m/m	BAS (2000)
Q_{melt}	1.1 - 7.4 mm/yr	$\pm$3 mm/yr	

TABLE 2 Table of parameter values and associated errors used in calculation of heat balance.

REFERENCES CITED

BAS (2000). A new ice thickness and subglacial topographic model of the antarctic.

Clark, P. U. and J. S. Walder (1994). Subglacial drainage, eskers, and deforming beds beneath the Laurentide and Eurasian ice sheets. *GSA Bullentin 106*(2), 304–314.

Comiso, J. C. (2000). Variability and trends in Antarctic surface temperatures from in situ and satellite infrared measurements. *Journal of Climate 13*, 1674–1696.

Creyts, T. T. and C. G. Schoof (2009). Drainage through subglacial water sheets. *Journal of Geophysical Research 114*(F04008), 1–18.

Flowers, G. E. (2010). Glacier hydromechanics: early insights and the lasting legacy of three works by iken and colleagues. *Journal of Glaciology 56*(200), 1069–1078.

Fountain, A. G. and J. S. Walder (1998). Water flow through temperate glaciers. *Reviews of Geophysics 36*(3), 299–328.

Glen, J. W. (1955). The creep of polycrystalline ice. *Proceedings of the Royal Society of London. Series A. Mathematical and Physical Sciences 228*, 519–538.

Hewitt, I. J. (2011). Modelling distributed and channelized subglacial drainage: the spacing of channels. *Journal of Glaciology 57*(202), 302–314.

Jezek, K., X. Wu, P. Gogineni, E. Rodriguez, A. Freeman, F. Rodriguez-Morales, and C. D. Clark (2011). Radar images of the bed of the Greenland Ice Sheet. *Geophysical Research Letters 38*(L01501), 1–5.

Joughin, I., J. L. Bamber, T. Scambos, S. Tulaczyk, M. Fahnestock, and D. R. MacAyeal (2006). Integrating satelite observations with modelling: basal shear stress of the Filcher-Ronne ice streams, Antarctica. *Philosophical Transactions of the Royal Society 364*, 1795–1814.

Kamb, B. (1991). Theological nonlinearity and flow instability in the deforming bed mechanism of ice stream motion. *Journal of Geophysical Research 96*(B10), 16585–16595.

Kamb, B., C. F. Raymond, W. D. Harrison, H. Engelhardt, K. A. Echelmeyer, N. Humphrey, M. M. Brugman, and T. Pfeffer (1985). Glacier surge mechanism: 1982-1983 surge of Variegated Glacier, Alaska. *Science 227*(4686), 469–479.

Lliboutry, L. (1964). Sub-glacial 'supercavitation' as a cause of the rapid advances of glaciers. *Nature 202*(4927), 77.

Nienow, P. W., M. Sharp, and I. C. Willis (1996). Velocity-discharge relationships derived from dye tracer experiments in glacial meltwaters: Implications for subglacial flow conditions. *Hydrological Processes 10*, 1411–1426.

Nye, J. F. (1976). Water flow in glaciers: Jokulhlaups, tunnels, and veins. *Journal of Glaciology 17*(76), 181–207.

Pimentel, S. and G. E. Flowers (2011). A numerical study of hydrologically driven glacier dynamics and subglacial flooding. *Proceedings of the Royal Society A 467*, 537–558.

Rempel, A. W. (2009). Transient effective stress variations forced by changes in conduit pressure beneath glaciers and ice sheets. *Annals of Glaciology 50*(52), 61–66.

Rignot, E., J. Mouginot, and B. Scheuchl (2011). Ice flow of the Antarctic Ice Sheet. *Science 333*, 1427–1430.

Rothlisberger, H. (1972). Water pressure and intra- and subglacial channels. *Journal of Glaciology 11*(62), 177–203.

Schoof, C. (2005). The effect of cavitation on glacier sliding. *Proceedings of the Royal Society of London, Ser. A 461*(2055), 609–627.

Schoof, C. (2010). Ice-sheet acceleration driven by melt supply variability. *Letters to Nature 468*, 803–806.

Shapiro, N. M. and M. H. Ritzwoller (2004). Inferring surface heat flux distributions guided by a global seismic model: particular application to antarctica. *Earth and Planetary Science Letters 223*, 213–224.

Walder, J. S. (1982). Stability of sheet flow of water beneath temperate glaciers and implications for glacier surging. *Journal of Glaciology 28*(99), 273–293.

Walder, J. S. and A. Fowler (1994). Channelized subglacial drainage over a deformable bed. *Journal of Glaciology 40*(134), 3–15.

Weertman, J. (1972). General theory of water flow at the base of a glacier or ice sheet. *Reviews of Geophysics and Space Physics 10*(1), 287–333.